

**Actin subunit structural diversity in Sonic Hedgehog
medulloblastoma:
implications for cancer biology and neurodevelopment**

Jamie Beaulieu

Integrated Program in Neuroscience, McGill University, Montréal

July 2022

A thesis submitted to McGill University in partial fulfilment of the requirements of the degree of
Master of Science

© Jamie Beaulieu 2022

Abstract

Actin is one of the most abundant proteins found in cells and has been linked to a wide range of cellular functions. Despite having more than a century of documentation on actin form and function, the identification and characterization of each subunit is a relatively recent achievement. As such, much remains to be studied on the individual roles and biochemical interactions of isoforms, especially in a disease setting. Alpha-cardiac actin (ACTC1) is one of 6 actin isoforms. It is mainly expressed in cardiac tissue and as such, its mutated forms have been tightly linked to congenital heart defects in humans.

Interestingly, the ACTC1 subunit has been shown to be overexpressed in both glioblastoma (GBM) and medulloblastoma (MB), two types of brain cancer. In Sonic Hedgehog (SHH) subtype MB, its overexpression has been linked to increased cell survival, migration, and resistance to mitotic inhibition. However, the mechanisms by which it confers these tumorigenic advantages remains unknown. Better understanding these biochemical interactions will be critical in enabling the development of new therapeutics or diagnostic tools that can leverage ACTC1's overexpression in MB. In this study, we successfully demonstrated that ACTC1 is a major constituent of F-actin and that alterations in its expression impacts both stress fiber length and abundance. ACTC1 was also shown to form complexes with both ACTG1 and ACTB subunits in F-actin and this unique actin subunit structural diversity is a defining feature of mitotic inhibitor resistance by SHH MB. We further demonstrated that ACTC1 is highly expressed in early post-natal mouse granule neuron progenitor cells, the cell of origin of SHH MB, which suggests it also has implications for normal neurodevelopment.

Taken together, these results represent the first step in characterizing the mechanism of action of ACTC1 in SHH MB. Additionally, this data has opened the door for further investigation of the role of ACTC1 in early neurodevelopment.

Résumé

L'actine est l'une des protéines les plus abondantes retrouvées dans les cellules et a été liée à un large éventail de fonctions cellulaires. Malgré plus d'un siècle de documentation sur la forme et la fonction de l'actine, l'identification et la caractérisation de chaque sous-unité est une réalisation relativement récente. À ce titre, il reste encore beaucoup à étudier sur les rôles individuels et les interactions biochimiques des isoformes, en particulier dans un contexte pathologique. L'actine alpha-cardiaque (ACTC1) est l'une des 6 isoformes d'actine. Il est principalement exprimé dans le tissu cardiaque et, à ce titre, ses formes mutées ont été étroitement liées aux malformations cardiaques congénitales chez l'homme.

Il est donc intéressant de constater que la sous-unité ACTC1 est surexprimée à la fois dans le glioblastome (GBM) et le médulloblastome (MB), deux types de cancer du cerveau. Dans le MB de sous-type Sonic Hedgehog (SHH), sa surexpression a été liée à une augmentation de la survie cellulaire, de la migration et de la résistance à l'inhibition mitotique. Cependant, les mécanismes par lesquels il confère ces avantages tumorigènes restent inconnus. Une meilleure compréhension de ces interactions biochimiques sera essentielle pour permettre le développement de nouveaux outils thérapeutiques ou diagnostiques pouvant tirer parti de la surexpression d'ACTC1 dans MB. Dans cette étude, nous avons démontré avec succès que l'ACTC1 est un constituant majeur de la F-actine et que des altérations de son expression ont un impact à la fois sur la longueur et l'abondance des fibres de stress. Il a également été démontré que ACTC1 forme des complexes avec les sous-unités ACTG1 et ACTB dans la F-actine et cette diversité structurelle unique de sous-unités d'actine est une caractéristique déterminante de la résistance aux inhibiteurs mitotiques

par le MB SHH. Finalement, nous avons démontré que l'ACTC1 est fortement exprimée dans les cellules progénitrices de neurones granulaires de souris postnatales, la cellule d'origine du MB SHH, ce qui suggère qu'elle a également des implications pour le développement neurologique normal.

Pris ensemble, ces résultats représentent la première étape dans la caractérisation du mécanisme d'action d'ACTC1 dans le MB SHH. De plus, ces données ont ouvert la porte à une enquête plus approfondie sur le rôle de l'ACTC1 dans le développement neurologique.

Table of Contents

ABSTRACT	I
RÉSUMÉ	III
TABLE OF CONTENTS	V
LIST OF TABLES	VII
LIST OF FIGURES	VIII
LIST OF ABBREVIATIONS	IX
PREFACE	II
ACKNOWLEDGEMENTS	III
INTRODUCTION	1
Role of actin in cell and cancer biology	1
Biochemistry	1
Actin dynamics	2
F-actin organization	3
Importance of actin isoforms	4
Role of actin in cancer	5
ACTC1 and cancer	7
Actin subunit expression in medulloblastoma	8
Medulloblastoma and neurodevelopment	10
Medulloblastoma	10
SHH medulloblastoma subgroup	10
Shh signaling and oncogenesis	11
Aurora kinase B inhibition	12
Congenital heart disease and ACTC1	13
Linking neurodevelopmental disorders to congenital heart disease	14
RATIONALE FOR STUDY	16
AIMS AND HYPOTHESIS	16
METHODS	18
Cell culture	18
Post-natal granule neuron progenitor cell isolation	18
Western blot	19
Immunofluorescence	20
F-/G-actin fractionation	21
F/G assay	22

F/G stress assay	22
Co-immunoprecipitation	23
Creation of Stable ACTC1-Overexpression Line	24
Transient shRNA ACTC1 knockdown	24
Stress fiber analysis	24
ACTC1 Analysis in Published Medulloblastoma Tumor Datasets	25
Statistics	25
RESULTS	26
Aim (1) – To assess the sub-cellular localization and co-polymerization of ACTC1 with other actin subunits in medulloblastoma.	26
Aim (1.1) – Identification of actin subunit protein expression across different SHH MB cell lines	26
Aim (1.2) – Quantification of actin subunit F/G ratios in SHH MB	29
Aim (1.3) – Determination of actin subunit co-localization with F-actin	31
Aim (1.4) – Determination of ACTC1 co-localization with other actin subunits	31
Aim (1.5) – Determination of ACTC1 complex formation with individual actin subunits	34
Aim 2 – To assess the effect of ACTC1 expression on stress fiber composition in SHH medulloblastoma	36
Aim (2.1) – Quantification of stress fiber length distribution and total fiber length following either ACTC1 KD or OE	36
Aim 3 – To determine whether F/G ratios are maintained during mitotic inhibition in SHH medulloblastoma resistant to apoptosis induced by Aurora kinase B inhibition.	38
Aim (3.1) – Quantification of SHH MB ACTC1 F/G ratio shifts following treatment with the mitotic inhibitor AZD1152	38
Aim 4 – To assess the expression of ACTC1 in mice post-natal granule neuron progenitors.	40
Aim (4.1) – Determination of ACTC1 protein expression in early post-natal mouse cerebellum	40
Aim (4.2) – Determination of ACTC1 protein expression in GNPs	42
Aim (4.3) – Quantification of granule neuron progenitor extraction purity from mouse cerebellum	44
DISCUSSION	46
ACTC1 co-localizes and forms complexes with both non-muscle actin isoforms in F-actin	46
ACTC1 expression levels modify stress fiber composition in SHH cells	47
Maintenance of ACTC1 in F-actin is a defining feature of mitotic inhibitor resistance by SHH MB	48
ACTC1 is expressed in mouse granule neuron progenitor cells	49
CONCLUSION	52
APPENDIX 1. SUPPLEMENTARY INFORMATION	54
BIBLIOGRAPHY	59

List of tables

Table 1. Actin isoforms and their tissue specific expression patterns in mammals.	2
Table 2: Western blot antibody list	53
Table 3: Immunofluorescence antibody list	54
Table 4: Parameter settings used for stress fiber analysis using the FSegment software	56

List of figures

Figure 1.	mRNA expression profiling for ACTG1, ACTG2, ACTB, ACTA1 and ACTA2.	2
Figure 1.	mRNA expression profiling of actin subunits in medulloblastoma subtypes.	9
Figure 2.	Western blots demonstrating actin isoform protein expression across different SHH MB cell lines	27
Figure 3.	Relative actin subunit protein expression levels across three different SHH MB cells lines.	28
Figure 4.	F/G ratios for ACTC1, ACTG1, ACTB and ACTA2 in UW426 SHH MB.	30
Figure 5.	Double-immunofluorescence imaging of ACTC1, ACTB, ACTG1 or ACTA2 with Phalloidin.	32
Figure 6.	Double-immunofluorescence imaging of ACTB, ACTG1 or ACTA2 with ACTC1.	33
Figure 7.	Co-immunoprecipitation of ACTG1 and ACTB with ACTC1 in UW426 SHH MB.	35
Figure 8.	Stress fiber length distribution and total fiber length following either ACTC1 KD or OE.	37
Figure 9.	UW426 ACTC1 F/G ratio in response to Aurora kinase B inhibition at two different time points.	39
Figure 10.	Western blot showing ACTC1 expression in post-natal day 1 mice whole cerebellum.	41
Figure 11.	Western blot analysis of ACTC1 expression in mouse granule neuron and progenitor cells.	43
Figure 12.	Co-immunofluorescence imaging of ACTC1 expression in granule neuron progenitor cells.	45
Figure 13.	Image processing for stress fiber quantification.	57

List of abbreviations

22q11.2DS: 22q11.2 deletion syndrome

ABP: actin binding protein

ACTA1: α_{skeletal} -actin 1

ACTA2: α_{smooth} -actin 2

ACTB: β_{cyto} -actin

ACTC1: α_{cardiac} -actin 1

ACTG1: γ_{cyto} -actin 1

ACTG2: γ_{smooth} -actin 2

ADF: actin depolymerizing factor

ASD: atrial-septal defects

Cc: critical concentration

CHD: congenital heart disease

CNS: central nervous system

DCM: dilated cardiomyopathy

EGF: epidermal growth factor

EGL: external granule layer

EMT: epithelial-to-mesenchymal transition

F-actin: filamentous actin

FRET: Förster resonance energy transfer

G-actin: globular actin

GBM: glioblastoma

GNP: granule neuron progenitor

IGL: internal granule layer

KD: knockdown

KO: knockout

MB: medulloblastoma

MT: myosin-tropomyosin

NDDs: neurodevelopmental disorders

NEPs: Nestin-expressing progenitors

NFs: nucleating factors

***PTCH1*:** patched 1 homologue

SHH: sonic hedgehog

***SMO*:** smoothed

SRF: serum response

***SUFU*:** suppressor of fused homologue

TGF- β : transforming growth factor beta

TME: tumor microenvironment

WNT: wingless

Preface

Jamie Beaulieu conducted the literature review, performed experiments and analyses, and wrote the thesis. Dr. Roberto Diaz conceived of the project, provided supervision, and reviewed the thesis. Rahul Suresh and Rita Lo provided protocols and methodological training. Dr. David Knapp provided help with experimental design, protocols, and reagents.

Acknowledgements

The past two years would have not been possible without the help of many people.

I'd first like to thank my supervisor Dr. Roberto Diaz, for welcoming me into his lab amid a global pandemic and supporting me throughout my project. Despite your crazy schedule and the logistical complications of the COVID-19 pandemic, you always found a time to meet when I needed advice on an experiment, and you took the time to solve problems with me when they arose. Your mentorship means a great deal to me and I'm glad I was able to learn from you during these last two years.

Thank you to Dr. David Knapp for teaching me a multitude of basic lab skills only a few months before starting my master's degree. Your expertise provided me with a great toolkit to accelerate my own work and has propelled me much further than I could have ever imagined. Thank you for also being a point of reference along my studies and providing me with valuable advice to advance my scientific career.

Thank you to former Diaz lab member Rahul Suresh and members of the McPherson lab for valuable knowledge transfer and helpful conversations.

Thank you to my committee members, Dr. Alanna Watt, Dr. Arnold Ludwig-Hayer and Dr. Nathalie Lamarche-Vane for your advice and recommendations during my committee meetings.

Thank you to Dr. Gary Armstrong for being my M.Sc. mentor and providing me with impactful words of encouragement. You've motivated me to keep pursuing science as hard as it may be.

Finally, thank you to all my friends and family who have always believed in me. You've all pushed me to keep thinking big and your words of encouragement are what fuel my daily drive. I couldn't have made it without you.

1 **Introduction**

2

3 **Role of actin in cell and cancer biology**

4

5 **Biochemistry**

6 Actin is one of the most abundant proteins found in eukaryotic cells and performs many functions
7 ranging from cell motility to vesicle trafficking and chromatin remodeling¹⁻³. Actin weighs 42 kDa
8 and is highly conserved even between different vertebrate species going from birds to mammals⁴.
9 It is also involved in more protein-protein interactions than any other known protein⁵. Vertebrates
10 express 6 actin isoforms which differ slightly at their N-terminal amino acid sequence but it is still
11 unclear whether these changes account for their unique functions^{5,6}. β_{cyto} -actin (ACTB) and γ_{cyto} -
12 actin 1 (ACTG1) are ubiquitously expressed in mammalian cells and share the highest sequence
13 identity while α_{skeletal} -actin 1 (ACTA1), α_{smooth} -actin 2 (ACTA2), α_{cardiac} -actin 1 (ACTC1), and γ_{smooth} -
14 actin 2 (ACTG2) are almost exclusively reserved to muscle cells⁵ (**Table 1**). The tissue specificity
15 of of the actin isoforms has been validated by expression profiling and knockout (KO)/knockdown
16 (KD) experiments. In addition to the slight nucleotide differences of actin subunits, actin
17 monomers can undergo post-translational modifications such as methylation and acetylation which
18 contributes to filament heterogeneity and alters their interaction with other proteins and small
19 molecules⁷. These changes are believed to be important in enabling isoform-specific cellular roles.

20

21

22

23

1 **Table 1. Actin isoforms and their tissue specific expression patterns in mammals.**

Name	Gene	Primary tissue specificity	Reference
β -cytoplasmic actin	<i>Actb</i>	Ubiquitous	8,9
γ -cytoplasmic actin	<i>Actg1</i>	Ubiquitous	10,11
γ -enteric smooth muscle actin	<i>Actg2</i>	All smooth muscle (except small blood vessels)	12–14
α -cardiac actin	<i>Actc1</i>	Heart	15
α -skeletal actin	<i>Acta1</i>	Striated muscle	16,17
γ -smooth muscle actin	<i>Acta2</i>	All smooth muscle including blood vessels	18,19

2

3 **Actin dynamics**

4 The ability of actin to perform its range of cellular functions is primarily attributable to the constant
5 shift between the monomeric globular state (G-actin) and the polymerized filamentous state (F-
6 actin), and through interactions with hundreds of actin-binding proteins (ABPs)²⁰. Filament (dis-
7)assembly is under the tight control of ABPs and small molecules. Polymerization of actin occurs
8 through the addition of the more stable ATP-bound monomers onto the growing barbed (+) end of
9 the filament while depolymerization is promoted by ATP-hydrolysis leading to dissociation of
10 ADP-bound monomers at the “-” end. In vivo nucleation, or initiation of F-actin formation,
11 requires the help of the Arp2/3 complex which also serves to stabilize actin branched networks²¹.
12 Formins are a class of ABPs which are instrumental in enhancing the nucleation of actin filaments
13 as well as regulating the rate of elongation²². Profilin is a another ABP which serves to add ATP-
14 bound monomers to growing F-actin strands²¹. On the other hand, actin depolymerizing factors
15 (ADFs) such as proteins of the cofilin family are responsible for fine-tuning the rate of G-actin

1 turnover by dissociation of ADP-bound monomers at the “-” ends. Additional ABPs such as
2 tropomyosin, gelsolin and CapZ can interact with F-actin to further regulate polymerization
3 dynamics²³. For example, in neurons gelsolin and cofilin are involved in apoptosis signaling
4 through breakdown of F-actin^{24,25}. More broadly, the actin cytoskeleton is known to reorganize
5 into a peripheral actomyosin cortical ring during apoptosis²⁶. Dynamic membrane protrusions
6 (blebs) form by differential pressure gradients caused by weakened actin cytoskeleton interactions
7 with the plasma membrane. Blebs can then attract phagocytic monocytes by chemotaxis²⁷. Thus,
8 actin and ABPs have been clearly defined as a central components of both intrinsic and extrinsic
9 apoptotic signaling pathways, but the role of isoform composition in dysregulating apoptosis
10 signaling in cancer is still unknown^{28,29}.

11

12 **F-actin organization**

13 As actin monomers polymerize to form F-actin strands, these filaments can give rise to different
14 types of organization that will serve unique functions within the cell. Branched networks are the
15 first type of organization. They mainly form at the leading edge and serve to enable cell motility
16 and shape changes by formation of structures like lamellipodium³⁰. They also play an important
17 role at the site of clathrin-mediated endocytosis and for meiotic spindle positioning^{31,32}. The F-actin
18 organizes into shorter but highly branched networks to allow for greater force generation. The
19 Arp2/3 complex is critical in initiating these branched networks and capping proteins make sure
20 filament growth is limited. On the other hand, crosslinked actin networks are defined as any actin
21 networks that rely on cross-linking proteins excluding the Arp2/3 complex required for initiation³⁰.
22 These networks are involved in controlling cell shape and mechanical integrity. Crosslinked
23 networks are a mixture of entangled and bundled filaments that work to prevent a linear

1 viscoelastic response to force. In other words, they allow the cell to resist physical stress that may
2 cause damage. Parallel actin bundles are the third type of network. They form filipodia, microvilli
3 and hair cells³³⁻³⁵. As their name implies, they are made of filaments in which the barbed ends are
4 in the same orientation. These bundles usually form by uncapping of branched filaments which
5 elongate in the same direction. Finally, antiparallel actin structures are essential for stress fiber
6 function and cytokinesis³⁰. This configuration allows for contraction of fibers when bundled with
7 myosin. The stress fibers mentioned above are useful for mechanosensing and supporting
8 lamellipodium motility^{36,37}. Their ability to contract is also believed to be used to crush the actin
9 network and accelerate its disassembly³⁸.

10

11 **Importance of actin isoforms**

12 Given their high sequence similarity but marked differential expression across cell types,
13 individual actin isoforms have been extensively researched in the last decade. KO experiments
14 were conducted on actin isoforms to better understand their unique roles. Loss of ACTC1, ACTCB
15 or ACTCA1 was shown to be lethal whereas KO of ACTG1, ACTG2 or ACTA2 led to viable
16 organisms but with severe developmental defects^{10,39-43}. However, these results may not directly
17 translate to humans as subunit expression patterns are not always consistent across species which
18 complicates interpretation. Additionally, rescue assays leveraging the overexpression of a different
19 isoform were only capable of showing partial regain of function⁴¹. These results were consistent
20 with studies which observed that muscle actins are not interchangeable with non-muscle actins in
21 intracellular structures^{44,45}. This suggests that their slight amino acid differences are enough to
22 induce significant functional changes. Therefore, to conduct such a vast array of cellular tasks,
23 polymerized actin must rely on a balanced and precisely controlled subunit diversity⁴⁶. One way

1 it could be achieving this is by leveraging differences in mRNA coding regions between isoforms
2 which affects translation dynamics, and in turn post-translational modifications that further
3 regulate fiber polymerization and architecture^{47,48}.

4
5 Some theories arising from experimental observations have suggested that the mechanistic
6 explanation for the distinct functionalities of actin isoforms could be their unique affinities for
7 ABPs or by their differential integration into F-actin⁶. Researchers have tried testing these
8 assumptions in various ways. For example, experiments on in vitro cultured muscle and non-
9 muscle cells have demonstrated that the unique ratio of copolymerized actin isoforms differs based
10 on both cell type and subcellular location of protein synthesis⁴⁹. Other studies looking exclusively
11 at non-muscle actin interactions (ACTB and ACTG1) using Förster resonance energy transfer
12 (FRET) showed that they have the ability to copolymerize⁵⁰. However, little data has been
13 provided for the interactions between other subunits so heteropolymer formation remains a
14 question to be fully answered. In vitro studies have not yet been able to fully recapitulate the
15 mechanism of in vivo polymerization while in vivo studies have not been able to produce
16 convincing data for different isoform polymerization into a single filament. Overall, these findings
17 support the idea that actin isoforms serve for the most part non-redundant roles and that their
18 relative diversity is important for defining cytoskeletal form and function.

19 20 **Role of actin in cancer**

21 Given the importance of the actin cytoskeleton in cell survival, migration and proliferation, its role
22 in cancer has also been widely investigated^{1,51,52}. Actin and ABPs have been found to be implicated
23 in virtually all steps of carcinogenesis. Cancer cells undergo a series of mutations which eventually

1 grant them phenotypic advantages commonly defined as “Hallmarks of cancer”⁵³. These traits
2 often rely on cytoskeletal rearrangements/interactions. For example, abnormal signaling cues
3 controlled and executed by the actin cytoskeleton can lead to the invasion and metastatic spread
4 of malignant cells⁵⁴. Often, it is the ABPs which regulate normal cytoskeletal function that become
5 aberrantly expressed and indirectly enhance invasive phenotypes^{51,55}.

6

7 Actin can form a multitude of structures which are known to facilitate cell migration and invasion
8 in cancer. The most common are: 1) lamellipodia and filipodia which form at the leading edge and
9 propel the cell in a specific direction, 2) invadopodia which help to pierce through the epithelium
10 and basal membrane upon receiving environmental cues and form secondary tumours and 3)
11 protruding blebs formed by cortex reorganization which facilitate amoeboid-like migration⁵⁶.
12 Furthermore, investigations of secondary tumour sites have revealed that metastatic cancer cells
13 exhibit a phenomenon closely related to epithelial-to-mesenchymal transition (EMT) which
14 promotes migratory potential and invasiveness⁵⁷. The EMT is known to be enabled by actin
15 dynamics which has pushed scientists to further investigate actin’s role in cancer migration^{58–60}.

16

17 Additionally, cancer cells heavily rely on perturbations in G-actin turnover to promote actin
18 architecture reorganization. These changes in actin dynamics often result from a shift towards or
19 away from specific actin regulatory proteins. Nucleating factors (NFs) is one type of regulatory
20 protein which can become aberrantly expressed and lead to alterations in actin architectures,
21 responses to mitotic stress and migration potential^{61,62}. The formins are a major family of NFs that
22 regulate the formation of linear actin filaments and stabilize microtubules⁶³. These proteins are
23 also known to be implicated in cancer progression. Overall, having many proteins/molecules

1 interacting with the cytoskeleton equips cancer with a diverse set of control points to initiate and/or
2 enhance its survival, migration, and proliferation.

3

4 **ACTC1 and cancer**

5 Despite the extensive body of work covering ABPs and actin dynamics in cancer, the intricacies
6 of actin subunit composition have been largely neglected^{52,64,65}. Bioinformatic analyses have
7 revealed that aberrant actin subunit expression is a defining feature of many cancers, with distinct
8 functional effects dependent on both isoform and cell type⁶⁶⁻⁶⁹. The mechanisms of action
9 describing each subunit's implication in cancer have been previously reported but remain
10 unexplored for ACTC1. Interestingly, abnormal ACTC1 expression has been linked to increased
11 cell survival, migration, proliferation and chemoresistance various types of cancer^{68,70,71}. These
12 include head and neck, urothelial, and prostate cancer⁷²⁻⁷⁴. Furthermore, ACTC1 expression was
13 found to be upregulated in multi-drug resistant breast cancer cells⁷¹. Taxanes which are
14 microtubule-binding inhibitors of mitosis were determined to disturb normal ACTC1 gene
15 expression in lung and breast cancer^{75,76}. Another unusual finding is the presence of aberrant
16 ACTC1 expression in both MB and GBM^{68,70}. Ohtaki et al. reported that patients with tumours
17 expressing high levels of ACTC1 have shorter survival despite receiving radiation and alkylating
18 chemotherapy and overall, GBMs with high ACTC1 expression exhibit a more invasive
19 phenotype⁶⁸. Alternatively, in vitro siRNA KD of ACTC1 in the U87 GBM cell line inhibited
20 migration⁷⁷.

21

22 Our laboratory has recently observed that SHH MB cells characterized by high ACTC1 expression
23 are resistant to apoptosis induced by inhibition of Aurora kinase B, a key protein kinase involved

1 in chromosome segregation⁷⁰. *ACTC1* was also found to be involved in the control of SHH MB
2 survival and migration. Despite these reports, the mechanism of action defining *ACTC1*
3 expression in MB and GBM is still not completely understood. More work is needed to better
4 understand both the direct and indirect players involved in aberrant *ACTC1* expression.

5

6 **Actin subunit expression in medulloblastoma**

7 Aberrant *ACTC1* mRNA expression in SHH and WNT MB led our group to investigate the
8 expression of the other 5 actin subunits. Our collaborator, Dr. Marc Remke from German Cancer
9 Research Centre, has revealed that the other non-cardiac actin subunits show subtle fold changes
10 in mRNA expression across MB subtypes (**Figure 1**). Given the highly dynamic and interactive
11 nature of actin, it would be of use to further investigate the relationships between actin subunits
12 and their possible co-polymerization in MB. Highest fold changes were found to be in *ACTG1*
13 and *ACTB*, the ubiquitously expressed isoforms, while *ACTA2*, *ACTA1* and *ACTG2*, the
14 remaining tissue-specific isoforms, showed lower fold changes than *ACTC1*.

15

16

17

18

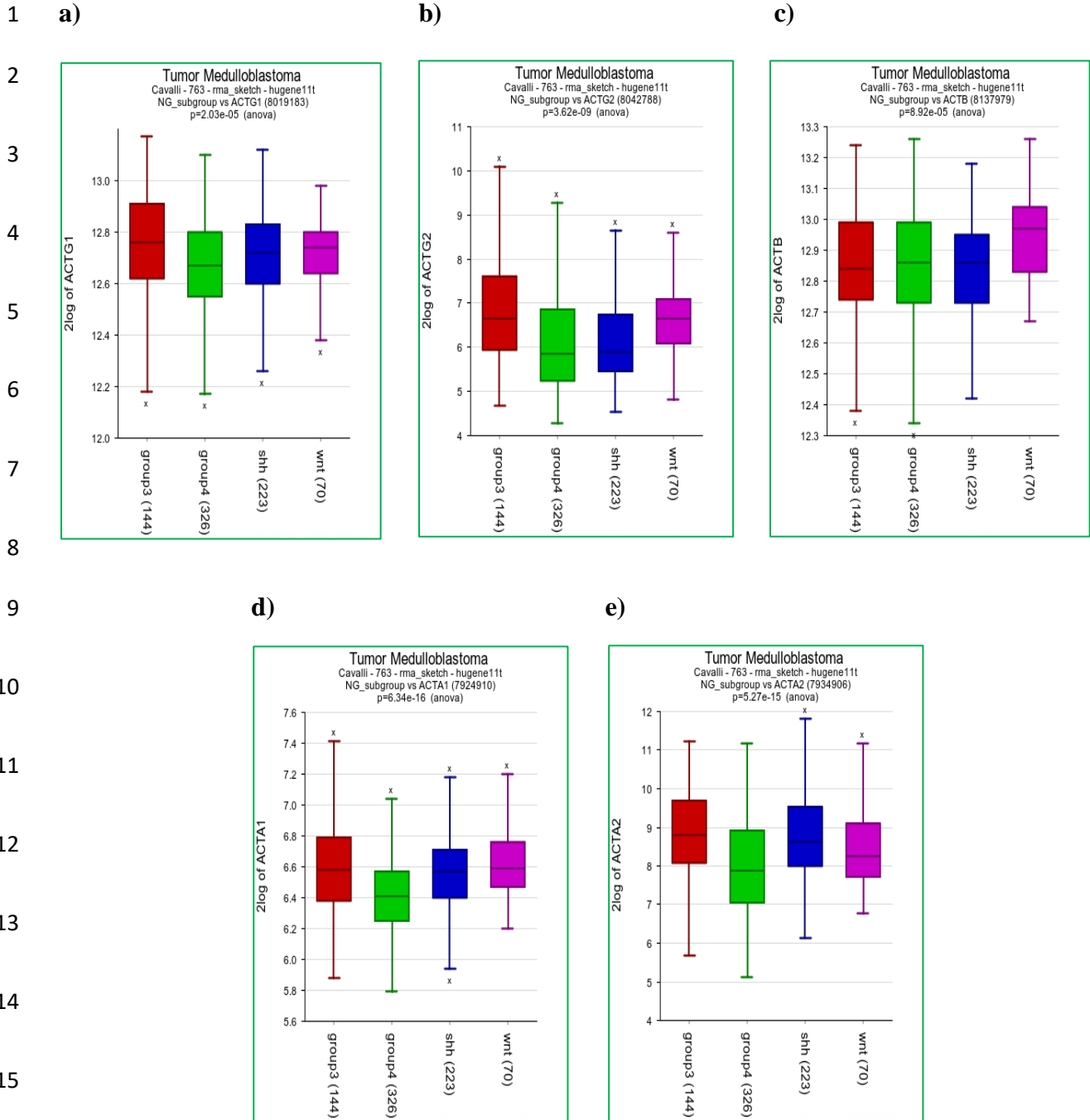
19

20

21

22

23



16 **Figure 1. mRNA expression profiling of actin subunits in medulloblastoma subtypes. a)**
 17 ***ACTG1*, b) *ACTG2*, c) *ACTB*, d) *ACTA1* and e) *ACTA2* mRNA expression log fold changes**
 18 **(n=763). (Unpublished, Dr. Marc Remke, German Cancer Research Centre, Dr. Florence Cavalli,**
 19 **Institut Curie).**

20

21

1 **Medulloblastoma and neurodevelopment**

2

3 **Medulloblastoma**

4 Medulloblastoma is the most common form of brain cancer in children. It is a primary central
5 nervous system (CNS) tumour that originates from embryonic cells in the cerebellum⁷⁸. MB is
6 comprised of four distinct molecular subgroups as reflected in the current revision of the WHO
7 classification: wingless (WNT), sonic hedgehog (SHH), group 3, and group 4⁷⁹. However, more
8 recent genomic analyses have uncovered deeper intertumoral heterogeneity within subgroups⁸⁰.
9 This further heterogeneity is mainly attributed to age groups and tumour aggressiveness. The
10 primary cause of MB-associated death is leptomeningeal metastasis which highlights the
11 importance of early diagnosis and treatment⁸¹. Current therapies for MB consist of surgical
12 resection of the tumour followed by cytotoxic chemotherapy and radiation which are known to
13 cause severe motor and cognitive impairments in young children⁸². Therefore, there is a necessity
14 for more personalized treatment regimens which can tailor toxicity levels to meet patients'
15 individual needs. Furthermore, recurrence of MB is almost always a fatal event. This underscores
16 the importance of developing a larger set of diagnostic tools for monitoring and treating MB.

17

18 **SHH medulloblastoma subgroup**

19 SHH MB is the most common subgroup accounting for over 30% of all MB cases⁸³. The SHH MB
20 subtype is characterized by aberrations in the sonic hedgehog signaling pathway which are
21 commonly caused by loss of function mutations of *PTCH1* (patched 1 homologue), *SUFU*
22 (suppressor of fused homologue) and *SMO* (smoothed)^{84,85}. These mutations lead to failure in
23 tumour suppression pathways and activation of Shh signaling with subsequent tumorigenesis. SHH

1 tumors are almost exclusively found in the cerebellum which is consistent with the localization of
2 granule neuron progenitors (GNPs), their cell of origin^{86,87}. Strong validation that SHH MB
3 originates from these cells was provided by deletion of *Ptch1* in mouse cerebellar GNPs which
4 resulted in MB formation with 100% penetrance⁸⁸. However, even if loss of *Ptch1* is necessary for
5 tumour formation, it is not sufficient in generating malignant transformation of cerebellar GNPs.
6 Most of the *Ptch1* deficient GNPs were able to differentiate on their own into the neuronal lineage
7 after prolonged culture⁸⁸. Therefore, it is likely that SHH MB tumorigenesis relies on dysregulation
8 of additional signaling pathways to seal its fate. Crosstalk with the Wnt, EGF and TGF- β pathways
9 have been shown and could likely be required for complete malignant transformation⁸⁹.

10

11 **Shh signaling and oncogenesis**

12 Shh is also known to be an important mitogen, morphogen and guidance molecule in normal CNS
13 organogenesis^{90,91}. It is considered a master player involved in patterning of the early post-natal
14 cerebellum. As such, Shh has been extensively studied for its role in GNP cell migration and
15 differentiation. Briefly, GNPs are thought to originate in the rhombic lip and migrate over to the
16 surface of the cerebellum to form the external germinal layer (EGL). Shh secreted by lower
17 Purkinje neurons helps promote GNP proliferation and migration towards the internal germinal
18 layer (IGL) where they ultimately differentiate into mature neurons^{92,93}. MB is believed to arise
19 from abnormal GNP proliferation somewhere early in this process. Other studies have recently
20 suggested that MB could derive from a rare population of lineage-restricted progenitors also
21 capable of generating granule cells⁹⁴. Unlike GNPs, these Nestin-expressing progenitors (NEP)
22 were found to reside in the deep part of the EGL and remain quiescent. Interestingly, this subgroup
23 was found to harbor reduced expression levels of DNA repair genes and, upon aberrant activation

1 of Shh signaling, showed significant increase in its ability to generate MB. It also did not express
2 Math1 (Atoh1), a neurogenic transcription factor considered essential for GNP to granule neuron
3 differentiation, which suggests they might be using an alternative maturation pathway. Overall,
4 these findings remind us that more efforts still need to be put towards understanding the
5 neurodevelopmental events implicated in MB formation.

6
7 Furthermore, recent reports focusing on the tumor microenvironment (TME) have highlighted the
8 importance of astrocytes in supporting SHH MB dissemination⁹⁵⁻⁹⁷. Astrocytes which support
9 proliferation and migration of GCPs under normal conditions have been shown to secrete Shh in
10 the TME, leading to Nestin expression in MB through a Smo-dependent but Gli1-independent
11 mechanism⁹⁵. Interestingly, part of the astrocytic population in the TME resulted from GCP
12 transdifferentiation which has never been recorded under normal physiological conditions⁹⁸. These
13 findings point towards the ever-increasing importance of the TME in MB progression and opens
14 new avenues for therapeutic development.

15
16 **Aurora kinase B inhibition**

17 Aurora kinase B (AURKB) is a mitotic serine/threonine protein kinase which is mutated in a
18 variety of cancers⁹⁹. Given its role in cell cycle progression, overexpression of AURKB is shown
19 to lead to tumor development, invasion and metastasis¹⁰⁰. Barasertib, also known as AZD1152, is
20 a potent and highly selective AURKB inhibitor which has become a novel drug candidate for
21 treating leukemia¹⁰¹. With the limited treatment options currently available for brain cancer, some
22 researchers have investigated whether AZD1152 could have a similar impact on CNS solid
23 tumours¹⁰². AZD1152 was shown to render Group 3 MB susceptible to apoptosis and growth

1 impairments¹⁰³. Interestingly, overexpression of ACTC1 in Group 3 MB which has the lowest
2 ACTC1 expression of all 4 MB subtypes led to abolition of apoptosis induced by AURKB
3 inhibition⁷⁰. Furthermore, SHH MB which shows the highest ACTC1 expression saw no
4 significant increase in cell death upon treatment with AZD1152 and overexpression of ACTC1 did
5 not induce any further changes. This suggests that high ACTC1 protein levels can provide cells
6 with protection from AURKB mitotic inhibitors, but the mechanism by which this occurs remains
7 unknown. It is of therapeutic interest to determine the protective role of ACTC1 to render SHH
8 MB susceptible to these mitotic inhibitors.

9

10 **Congenital heart disease and ACTC1**

11 ACTC1 is a major constituent of sarcomere thin filaments which are critical for the normal
12 function of the heart¹⁰⁴. Mutations in ACTC1 cause atrial-septal defects (ASD) associated with
13 late-onset dilated cardiomyopathy and hypertrophic cardiomyopathy which are classified as
14 congenital heart defects (CHD)^{15,105}. Given the high degree of sequence conservation for actin
15 genes, mutations in ACTC1 are a particularly interesting avenue to study CHD. Interestingly,
16 reduced ACTC1 expression has been linked to the onset of CHD by inducing cardiomyocyte
17 apoptosis¹⁰⁶. Alternatively, many studies have reported specific ACTC1 mutations which are
18 linked to ASD, but few have tried to investigate their effects on actin dynamics. The Y116C-ACTC
19 mutation is part of the myosin-tropomyosin (MT) class of mutations and is reported to lead to
20 polymerization deficiency through an increased critical concentration (Cc)^{107,108}. It was also shown
21 to reduce F-actin stability and create abnormal filament morphology but had no major impact on
22 actomyosin interactions¹⁰⁷. Through a genome-wide linkage analysis of a multi-generational
23 family, the G247D-ACTC mutation was identified in 15 family members affected with ASD but

1 absent in the remaining 63 healthy family members¹⁵. This heterozygous and nonsynonymous
2 mutations was shown to cause a loss-of-function phenotype in both human and neonatal rat
3 ventricular cardiomyocytes. Overexpression of this mutant protein led to structural defects in the
4 cytoskeleton, increased apoptosis, disrupted actin polymerization and caused sarcomeric disarray.
5 It was also found to negatively regulate serum response (SRF)-signaling, thereby contributing to
6 the late-onset dilated cardiomyopathy (DCM) observed in humans¹⁰⁹. Continued investigation of
7 the biochemical properties of mutated ACTC1 is likely to yield more valuable information about
8 the mechanisms governing CHD.

9

10 **Linking neurodevelopmental disorders to congenital heart disease**

11 Studies have shown that children with CHD are at greater risk of neurodevelopmental disorders
12 (NDDs)¹¹⁰. The latter includes cognitive, motor, behavioural, speech, and executive functioning
13 deficits, as well as autism spectrum disorder and psychiatric conditions. Degrees of
14 neurodevelopmental impairment vary in children with CHD, but effects can persist all the way into
15 adulthood. In addition, CHD and NDDs are both categorized as midline defects. Several theories
16 linking both diseases have been proposed over the years, but recent data suggests that mutations
17 in key genes could be the culprit¹¹¹. For example, the CHARGE syndrome is a complex genetic
18 syndrome highlighted by mutations in the CHD7 gene which encodes a chromodomain helicase
19 DNA binding protein¹¹². Phenotypic features are abundant with some of the most frequent being
20 developmental delays, cardiovascular malfunctions or other midline defects such as orofacial
21 clefts, genital hypoplasia and colobomas¹¹². The exact mechanisms by which CHD7 mutations
22 induce this vast array of abnormalities remains to be solved. Similarly, 22q11.2 deletion syndrome
23 (22q11.2DS) also has a heterogenous presentation as it can cause cognitive delays, psychiatric

1 illnesses, cardiac and palatal abnormalities to name a few¹¹³. In fact, 22q11.2DS is the most
2 common chromosomal microdeletion disorder and the second most common cause of CHD after
3 Down syndrome¹¹⁴. Researchers have pointed towards mutations in the TBX1 transcription factor
4 as being the origin for the suite of phenotypes ensuing¹¹⁵. These conditions are just a few out of
5 many which draw strong ties between CHD and neurodevelopmental impairments. Lots of work
6 remains to be done to provide a better explanation for these developmental abnormalities.

7

8

9

10

11

12

13

14

15

16

17

18

19

1 **Rationale for study**

2 SHH medulloblastoma, originating from GNPs in the EGL, has recently been shown to aberrantly
3 express ACTC1⁷⁰. Further investigation demonstrated that ACTC1 is linked to enhanced survival,
4 larger migratory ability and provides protection against mitotic inhibition. ACTC1 overexpression
5 has been described to have similar implications, particularly on migration potential, in other CNS
6 brain tumors such as glioblastoma⁷⁷. Given the importance of ACTC1 in modulating SHH MB
7 progression, it is of interest to further investigate the mechanisms by which ACTC1 enables these
8 oncogenic phenotypes. To do so, we first need to pinpoint ACTC1 in the context of actin dynamics.
9 This means studying its interactions with other actin isoforms such as ACTB, ACTG1 and ACTA2
10 which had the three next highest expression levels of all actin subunits (unpublished lab data). In
11 addition, contrasting these results with those found in GNPs will allow to better understand the
12 developmental implications of ACTC1.

13

14 **Aims and hypothesis**

15 We hypothesize that ACTC1 forms part of SHH MB F-actin and this polymerization contributes
16 to pro-survival and migratory signaling in SHH MB. Given that ACTC1 is not normally found in
17 mature neurons we propose that ACTC1 expression in MB may recapitulate a developmental
18 phenotype found in post-natal granule neuron progenitors. The aims of this study are:

19

20 (1) To assess the sub-cellular localization and co-polymerization of ACTC1 with other actin
21 subunits in SHH medulloblastoma.

22 i. Identification of actin subunit protein expression across different SHH MB cell
23 lines

- 1 ii. Quantification of actin subunit F/G ratios in SHH MB
- 2 iii. Determination of actin subunit co-localization with F-actin
- 3 iv. Determination of ACTC1 co-localization with other actin subunits
- 4 v. Determination of ACTC1 complex formation with individual actin subunits

5

6 (2) To assess the effect of ACTC1 expression on stress fiber composition in SHH
7 medulloblastoma

- 8 i. Quantification of stress fiber length distribution and total fiber length following
9 either ACTC1 KD or OE

10

11 (3) To determine whether F/G ratios are maintained during mitotic inhibition in SHH
12 medulloblastoma resistant to apoptosis induced by Aurora kinase B inhibition.

- 13 i. Quantification of SHH MB ACTC1 F/G ratio shifts following treatment with
14 the mitotic inhibitor AZD1152

15

16 (4) To assess the expression of ACTC1 in mice post-natal granule neuron progenitors.

- 17 i. Determination of ACTC1 protein expression in early post-natal mouse brain
- 18 ii. Determination of ACTC1 protein expression in GNPs
- 19 iii. Quantification of granule neuron extraction purity from mouse cerebellum

20

21

22

23

1 **Methods**

2

3 **Cell culture**

4 SHH subgroup MB cell lines UW426, UW228 and their derivatives were grown as adherent
5 cultures in Alpha modified Eagle's media (AMEM, Wisent) supplemented with 10% heat-
6 inactivated fetal bovine serum (FBS, Wisent, St. Bruno, QC, Canada). SHH subgroup DAOY cells
7 were grown as adherent cultures in Dulbecco's modified Eagle's medium (DMEM, Wisent, St.
8 Bruno, QC, Canada) supplemented with 10% heat inactivated FBS. Cells were incubated at 37°C
9 and 5% CO₂ atmosphere. Cells were passaged when 70-80% confluent using Trypsin 0.25%
10 EDTA (Gibco, Life Technologies, Burlington, ON, Canada). Post-natal granule progenitor cells
11 were cultured in NeuroCult™ Basal Medium (Mouse & Rat) (STEMCELL Technologies,
12 Vancouver, BC, Canada) supplemented with GlutaMAX™ (Gibco, Life Technologies,
13 Burlington, ON, Canada) and 2 M KCl. UW426, UW228 and DAOY cell lines were generously
14 provided by Dr. Annie Huang (Sick Kids Research Institute, Toronto, Canada). The DAOY cell
15 line was originally established from a biopsy of a solid tumor from a four-year-old male¹¹⁶. The
16 UW228 cell line and its derivatives were originally established from a biopsy of a solid tumor
17 from a nine-year-old female¹¹⁷. Granule neurons and progenitors were derived from C57BL/6 post-
18 natal mouse cerebellum provided by Dr. Abbas Sadikot (The Montreal Neurological Institute,
19 Montreal, Canada).

20

21 **Post-natal granule neuron progenitor cell isolation**

22 Isolation of post-natal cerebellar granule neuron progenitor cells was performed following the
23 protocol described by Lee et al.¹¹⁸. Briefly, post-natal day 3-8 mice were anesthetized on ice and

1 immediately after decapitated. Heads were fixed with small needles with the basal aspect
2 positioned upwards. The skull was cut with fine scissors starting from the anteriormost point of
3 the inferior margin of the foramen magnum, through the midline of the basioccipital, basisphenoid
4 and presphenoid bones of the skull and up until the middle of the palatine. The cut basal parts of
5 the skull were retracted to the sides to allow the medulla oblongata to rise. The cerebellum was
6 then carefully separated under the control of a dissecting microscope. The cerebellar tissue was
7 immediately placed in a cooled sterile HBSS-glucose solution. Once all the dissections were
8 finished, HBSS-glucose was removed and cerebellums were resuspended in a papain solution
9 made from the Papain Dissociation System kit (Fisher Scientific, Ottawa, ON, Canada). The
10 mixture was incubated at 37°C and 5% CO₂ atmosphere for 20min. Tissue was dissociated by
11 pipetting up and down 10 times. Suspended cells were transferred into a fresh tube, centrifuged,
12 and resuspended in DNase/albumin inhibitor solution. Cells were centrifuged in a discontinuous
13 density gradient made of f albumin-ovomuroid inhibitor solution. In order to further purify the
14 granule cell population, filtered cells were centrifuged in a Percoll density gradient made by
15 layering 60% Percoll solution underneath a 35% solution using a spinal needle. Cells at the
16 interface layer were collected, resuspended in serum media and pre-plated twice for 20 min. on a
17 poly-D-lysine-coated dish to allow larger non-granule cells to settle down and adhere. Cells were
18 then collected, spun down and resuspended in serum-free medium before being counted and
19 seeded for culture.

20

21 **Western blot**

22 Whole cell lysates were prepared using a modified RIPA buffer supplemented with a protease
23 inhibitor (cOmplete Mini protease inhibitor cocktail tablet, Roche, Laval, Canada). Rat lung and

1 mouse brain controls were obtained by flash freezing the dissected tissues in liquid nitrogen. They
2 were grounded up using a mortar and pestle and suspended in the modified RIPA lysis buffer.
3 Protein concentrations were determined using a BCA protein assay kit (PierceTM BCA Protein
4 Assay Kit, Thermo Fisher Scientific, Montréal, QC, Canada). Total proteins were run on 10%
5 SDS-PAGE gels and transferred onto nitrocellulose membranes using a semi-dry transfer
6 apparatus (Bio-Rad Laboratories, Hercules, CA, USA). Blocking was carried out using 1% non-
7 fat milk (BioShop Canada, Burlington, ON, Canada) in TBS-T (100 mM Tris-Cl, pH 8.1, 150 mM
8 NaCl, 0.1% Tween-20). Incubation of primary antibody (**Supplementary Table 2**) in TBS-T with
9 1% non-fat milk was performed at 4°C overnight. All wash steps were done using TBS-T.
10 Incubation of horseradish peroxidase-conjugated secondary antibody (**Supplementary Table 2**)
11 in TBS-T with 1% non-fat milk was performed for 1 hr, followed by enhanced chemiluminescence
12 detection. Enhanced chemiluminescence detection (PerkinElmer, Waltham, MA, USA) on
13 autoradiography film (Diamed Lab Supplies, Mississauga, ON, Canada) was used to detect
14 antibody signal. Equal protein loading was confirmed by re-probing blots for GAPDH.

15

16 **Immunofluorescence**

17 UW426 or granule cells (5×10^4 cells/well) were seeded on a sterile glass coverslip in triplicates.
18 Cells were allowed to grow for 2 days, reaching roughly 50% confluency on the coverslip. On the
19 day of the experiment, the growth medium was gently aspirated. Each well was washed twice with
20 PBS for 5 minutes. Under a fume hood, the cells were fixed to the coverslip by incubating with a
21 mixture of 3% paraformaldehyde (PFA) and 1.5% glutaraldehyde (GA) for 10-15 minutes. The
22 PFA-GA mix was then removed, and the coverslips were washed twice with PBS. At this stage,
23 the coverslips were either stored in 50% non-sterile glycerol in PBS at -20°C or moved on directly

1 to the next step. When coverslips went through freezer storage, two additional PBS washes were
2 performed. The coverslips were quickly moved to a moisture chamber covered with aluminium
3 foil and incubated in blocking solution consisting of 0.1% Triton X-100 (Sigma-Aldrich Canada,
4 Oakville, ON, Canada), 0.5% bovine serum albumin (Sigma-Aldrich Canada), and 5% normal
5 donkey serum in PBS for 1h. After 1h, blocking solution was gently aspirated using a vacuum and
6 primary antibody solutions (**Supplementary Table 3**) were added for overnight incubation at 4°C.
7 The next day, primary antibody solution was removed, and coverslips were washed twice with
8 blocking solution followed by PBS. Secondary antibodies (**Supplementary Table 3**) with or
9 without Alexa-fluor 647 Phalloidin stain (**Supplementary Table 3**) were diluted in PBS with 1%
10 BSA and incubated in the dark moisture chamber for 1.5h. After incubation, coverslips were
11 washed twice with blocking solution and PBS. Finally, Hoechst nuclear stain (**Supplementary**
12 **Table 3**) was added for 5 min. followed by two PBS washes. The coverslips were mounted on a
13 microscope slide using Fluormount-G (Southern Biotechnology Associates), dried in the dark
14 overnight and imaged using a Zeiss LSM700 confocal microscope with Zen Black 2010
15 acquisition software (Carl Zeiss, Oberkochen, Germany).

16

17 **F-/G-actin fractionation**

18 G-actin and F-actin fractions were isolated with the G-actin/F-actin in vivo assay kit (#BK037,
19 Cytoskeleton Inc.) using a modified version of the manufacturer's instructions. Briefly, media was
20 removed from wells. Cells were incubated in ice-cold lysis/F-actin stabilizing buffer supplemented
21 with protease inhibitor and ATP for 10 min. on ice. The lysate was then collected using a cell
22 scraper. Lysates were incubated for 20 min. on ice with frequent pipetting and centrifuged for
23 5 min. at $350 \times g$ to remove cell debris. 100ul of the cell lysate was centrifuged at $100,000 \times g$ for

1 1 h at 4 °C using an Optima TL-100 Ultracentrifuge (Beckman Coulter) with a TLA-100 fixed-
2 angle rotor. G-actin in the supernatant was transferred to a fresh tube while the F-actin in the pellet
3 was resuspended in 100 µl of F-actin destabilizing buffer for 1h on ice with frequent pipetting. G-
4 actin and F-actin fractions were mixed with 5X SDS sample buffer and stored at -20°C for
5 downstream analysis.

6

7 **F/G assay**

8 UW426 cells were seeded at 1.5×10^5 cells/well in a 6-well culture plate. Cells were grown for 2
9 days until roughly 80% confluent at the time of harvest. When the desired confluency was
10 reached, F-/G-fractions were collected following the F-/G-actin fractionation protocol. Equal
11 volumes (10ul) of F-/G-actin fractions were run on an SDS-PAGE gel for Western blot analysis
12 and probed using all 4 actin antibodies mentioned in **Supplementary Table 2**. F-/G-actin ratios
13 were determined by densitometry using FIJI/ImageJ software.

14

15 **F/G stress assay**

16 UW426 cells were seeded at 1×10^5 cells/well in a 6-well culture plate in technical triplicates. The
17 next day, the media in each well was substituted for either 100 nM AZD1152 (Selleck Chemicals
18 LLC, Houston, TX, USA) in media, 0.01% v/v dimethyl sulfoxide (DMSO, Sigma, St. Louis, MO,
19 USA) in media or media only. Cells were cultured in these conditions for 24h and 48h. When
20 harvest timepoints were reached, F-/G-fractions were collected following the F-/G-actin
21 fractionation protocol. Equal volumes (10ul) of F-/G-actin fractions were run on an SDS-PAGE
22 gel for Western blot analysis and probed using all 4 actin antibodies mentioned in **Supplementary**
23 **Table 2**. F-/G-actin ratios were determined by densitometry using FIJI/ImageJ software.

1 **Co-immunoprecipitation**

2 Co-immunoprecipitation samples were collected using the Dynabeads™ Protein G
3 Immunoprecipitation Kit (Thermo Fisher Scientific Baltics UAB, Vilnius, Lithuania) and the
4 Pierce™ Anti-DYKDDDDK Magnetic Agarose beads (Thermo Fisher Scientific, Rockford, IL,
5 USA) following manufacturer's instructions. Briefly for ACTC1 immunoprecipitation, 50ul of
6 Dynabeads™ was transferred to a 1.5ml tube for each UW426 F-fraction sample. Using a magnet,
7 the supernatant was removed and 1ug of Rabbit anti-ACTC1 Ab (Abcam; ab218549) in 200ul of
8 Ab Binding and Washing Buffer was added to the beads. The mixture was incubated with rotation
9 for 10 min. and washed once with Ab Binding and Washing Buffer. 90ul of each 100ul F-fraction
10 sample was diluted up to 200ul in Ab Binding and Washing Buffer which was used to resuspend
11 the beads. The remaining 10ul was diluted in 5X SDS sample buffer and kept as an input sample.
12 The F-fraction and bead mixture was incubated with rotation for 10 min., washed 3 times,
13 resuspended in Ab Binding and Washing Buffer and transferred into a fresh tube. ACTC1 and its
14 co-precipitated proteins were eluted in SDS sample buffer and boiled at 70°C for 10 min. Briefly
15 for FLAG immunoprecipitation, 50ul of slurry was transferred into a 1.5mL tube for each UW426
16 ACTC1 OE F-fraction sample. All wash steps were performed using complete F-actin stabilization
17 buffer (Cytoskeleton). 90ul of each 100ul F-fraction sample was diluted up to 200ul in complete
18 F-actin stabilization buffer which was used to resuspend the beads. The remaining 10ul was diluted
19 in 5X SDS sample buffer and kept as an input sample. The F-fraction and bead mixture was
20 incubated with rotation for 20 min., washed twice with buffer, once with purified water and finally
21 resuspended in SDS sample buffer. The samples were incubated 95°C for 10 min. The eluate was
22 separated from the beads using a magnet and ran on a 10% SDS-PAGE gel for Western blot
23 analysis.

1 **Creation of Stable ACTC1-Overexpression Line**

2 UW426 cells were transfected with plasmid DNA using Lipofectamine 2000 (ThermoFisher
3 Scientific). Forty-eight hours after transfection, selection was done using hygromycin at a
4 concentration of 250 µg/ml for 7 days. A single clone was then picked and expanded. The cells
5 were transfected with either a human ACTC1 overexpression plasmid containing a C-terminal
6 FLAG-tag (Ref.# HG10960-CF, Sino Biological), or an empty vector control. Expression of the
7 plasmid transgene was confirmed by Western blot (WB) analysis for the FLAG tag.

8

9 **Transient shRNA ACTC1 knockdown**

10 Approximately 7×10^5 UW426 cells were plated in a 6-well dish 24h before transfection.
11 Transfections were performed using Lipofectamine 2000 (ThermoFisher Scientific) reagent in a
12 1:2 (ug DNA to uL Lipofectamine) ratio in reduced-serum Opti-MEM medium (ThermoFisher
13 Scientific). Once a mixture of the DNA and reagent was created, it was added directly to the well
14 containing the complete media and UW426 cells and placed in a 37°C incubator. After 6 hours,
15 the media in the wells were changed to normal complete medium (AMEM with 10% FBS). The
16 cells were transfected with either an ACTC1 knockdown DNA plasmid (GeneCopoeia, Rockville,
17 MD, USA; Cat# HSH018117-CH1) or a scrambled control (GeneCopoeia; Cat# CSHCTR001-
18 CH1). The knockdown was confirmed by WB analysis.

19

20 **Stress fiber analysis**

21 Coverslips were prepared according to the immunofluorescence protocol above. The cells were
22 stained with Alexa-Fluor 647 nm fluorescent Phalloidin (ThermoFisher Scientific) and Hoechst
23 177 nuclear stain (ThermoFisher Scientific). Images were acquired using a Zeiss LSM700 confocal

1 microscope with Zen Black 2010 acquisition software (Carl Zeiss, Oberkochen, Germany). Stress
2 fibers were analyzed using FSegment (Universitätsmedizin Greifswald, Greifswald, Germany)
3 software in MATLAB Runtime (MathWorks, USA) according to the protocol by Rogge et al.²³
4 and using the parameters listed in **Supplementary Table 4**. Images of at least 150 cells were taken
5 for each cell line in three independent trials. 1 pixel length was equivalent to 0.1 μm in this setup.

6

7 **ACTC1 Analysis in Published Medulloblastoma Tumor Datasets**

8 Previously published gene expression data by Daniel Picard at the German Cancer Research Centre
9 were analyzed using R2 platform (<https://hgserver1.amc.nl/cgi-bin/r2/main.cgi>, Academic
10 Medical Center (AMC) Amsterdam, Netherlands)). Actin subunit expression was analyzed in
11 multiple medulloblastoma datasets (Heidelberg [PMID: 21911727], Pomeroy [PMID: 21098324],
12 Cavalli/Remke [PMID: 28609654], Kool [PMID: 18769486], and Gilbertson [PMID: 22722829])
13 by subgroups that were assigned in the original publication. The data found **Figure 1** is from the
14 Cavalli/Remke dataset only. However, other data sets which contain fewer tumour samples were
15 also explored and showed similar results. ANOVA was used to calculate significance.

16

17 **Statistics**

18 Prism 8 (GraphPad Software, Inc., CA, USA) was used for statistical analysis. All measures are
19 reported as mean \pm SE. Means were compared by independent samples Student's t-test. A P-
20 value $< .05$ was considered statistically significant. Unless otherwise indicated, all experiments
21 were averaged for 3 independent trials.

22

23

1 **Results**

2

3 **Aim (1) – To assess the sub-cellular localization and co-polymerization of ACTC1 with**
4 **other actin subunits in medulloblastoma.**

5 **Aim (1.1) – Identification of actin subunit protein expression across different SHH MB cell**
6 **lines**

7 Since *ACTC1* mRNA was shown to be significantly overexpressed in SHH MB cells, we sought
8 to measure the protein expression of actin subunits across the UW426, UW228 and DAOY SHH
9 MB cell lines. We chose to focus on ACTC1, ACTB, ACTG1 and ACTA2. The latter three
10 isoforms were shown to also have significant fold changes in mRNA expression (**Figure 1a, c and**
11 **e**). Since ACTB and ACTG1 are known to be ubiquitously expressed and generally have the largest
12 subunit protein expression levels in mammalian cells, they were good candidates to investigate co-
13 polymerization with ACTC1. Alternatively, ACTA2 had the next highest fold change in mRNA
14 expression for SHH MB of the remaining tissue-specific isoforms (**Figure 1e**). As expected,
15 Western blot analysis confirmed the expression of ACTC1, ACTB and ACTG1 across all three
16 SHH MB cell types (UW426, UW228 and DAOY) (**Figure 2**). However, ACTA2 was only
17 detected in UW426 and UW228 SHH cells (**Figure 2b**). Measurements of relative actin subunit
18 protein abundance was quantified across SHH MB cell lines (**Figure 3**). Although not significant,
19 ACTC1 had the highest expression in UW426 with a mean ACTC1/GAPDH density of 0.778.
20 Considering its relative ease of manipulation and considerable expression of all 4 actin subunits
21 being investigated, UW426 was chosen as a SHH MB model for subsequent experiments.

22

23

24

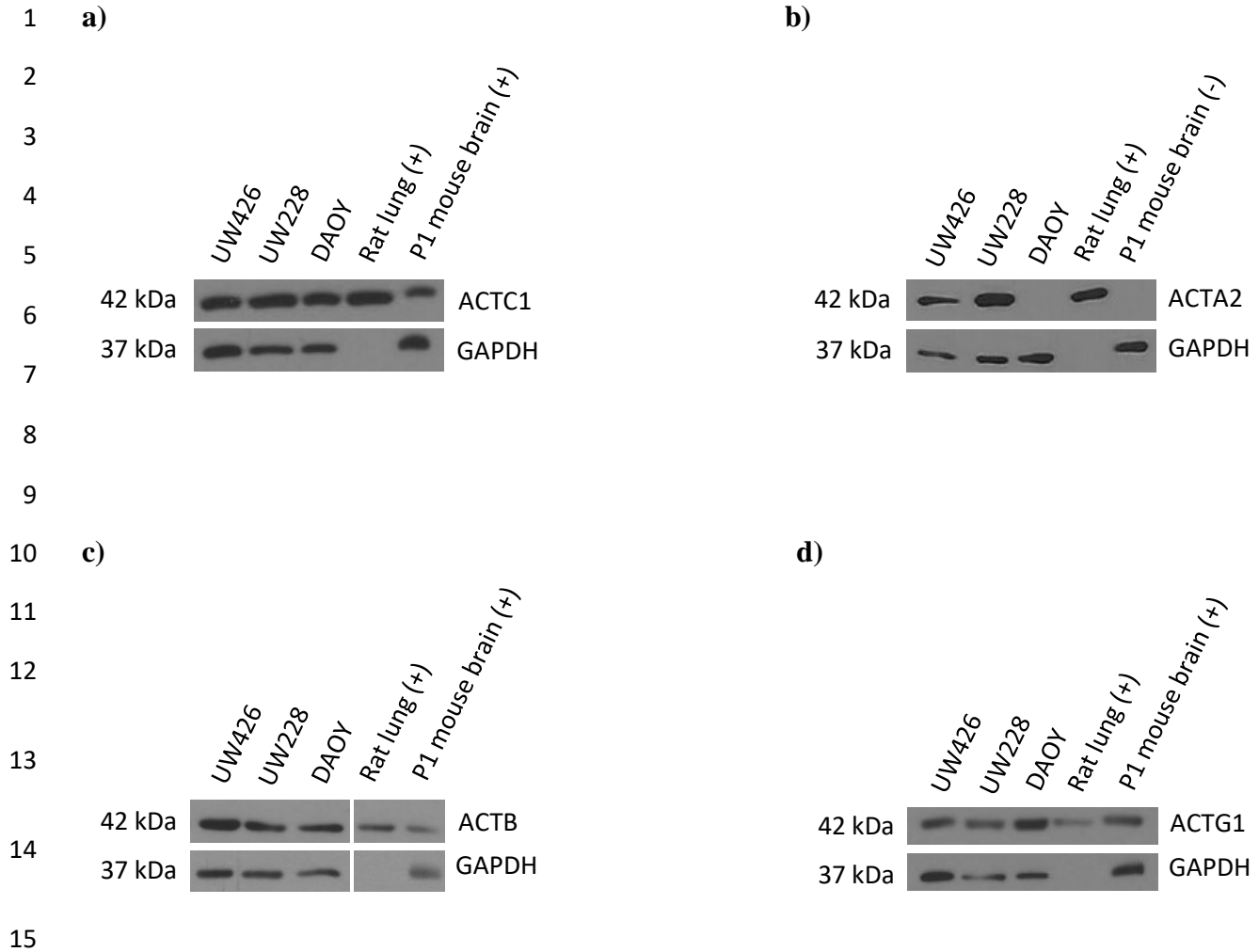
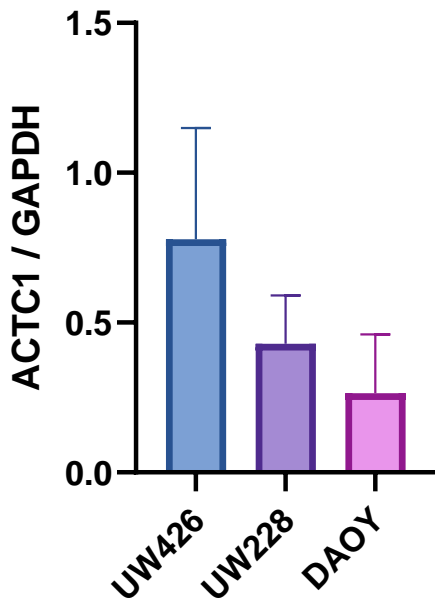


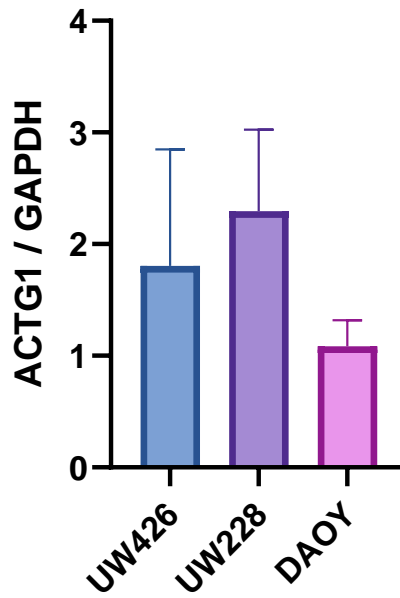
Figure 2. Western blots demonstrating actin isoform protein expression across different SHH MB cell lines. a) ACTC1, b) ACTA2, c) ACTB and d) ACTG1 protein expression. 5ug total protein loaded. Positive control (+) is rat lung for all actin subunits and early post-natal day 1 mouse whole brain for ACTC1, ACTB and ACTG1. Absence of a GAPDH band for the rat lung positive control is due to lower GAPDH levels in rat lung. Presence of ACTC1 in P1 mouse brain is explained by transient ACTC1 expression in early neurodevelopment. The ACTC1 antibody specificity was also validated using mouse heart (+) and liver (-) lysates not shown here (Rahul et al., 2021). Negative control (-) for ACTA2 subunit was early post-natal day 1 whole mouse brain lysate.

1

a)

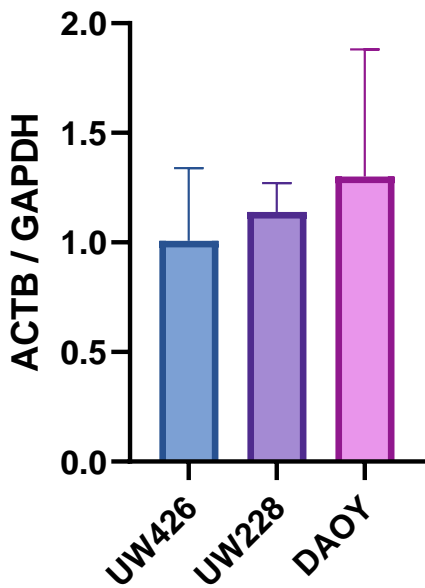


b)

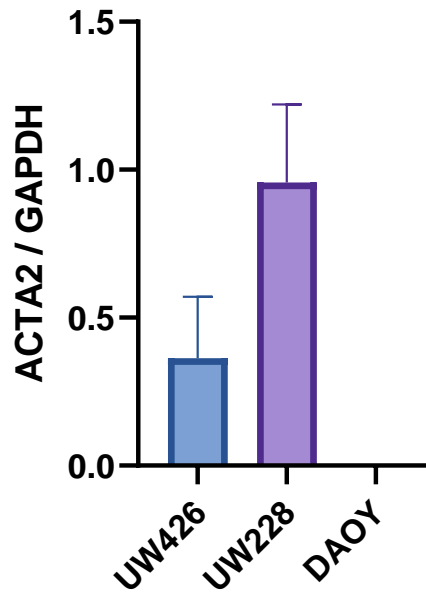


2

c)



d)



3

4 **Figure 3. Relative actin subunit protein expression levels across three different SHH MB**
5 **cells lines. a) ACTC1, b) ACTG1, c) ACTB and d) ACTA2 protein levels between UW426,**
6 **UW228 and DAOY SHH MB cells. Graphs represent mean of 3 biological replicates \pm SEM**
7 **quantified by densitometry from Western blots.**

1 **Aim (1.2) – Quantification of actin subunit F/G ratios in SHH MB**

2 We sought to investigate the relative distribution of ACTC1, ACTG1, ACTB and ACTA2 in F-
3 and G-actin from UW426 using an F/G ratio quantification assay. Western blot analysis showed
4 that all 4 actin isoforms were found to be expressed in both F- and G-actin fractions, although very
5 low amounts of ACTA2 were detected in F-actin (**Figure 4b**). Quantification of F/G ratios for
6 each actin subunit revealed a significantly elevated mean F/G ratio for ACTC1 (0.435 ± 0.0519)
7 and ACTG1 (0.517 ± 0.0464) relative to ACTA2 (0.062 ± 0.0242) (**Figure 4a**). Given the relative
8 instability of F-actin and its highly dynamic nature, the F/G ratio represents a much more accurate
9 measure of comparison between subunits than absolute fraction measurements. For this reason, we
10 chose to solely focus on F/G ratio quantification results to guide further experimental design.

11
12
13
14
15
16
17
18
19
20
21
22
23
24

1
2
3
4
5
6
7
8
9
10
11
12
13
14
15
16
17

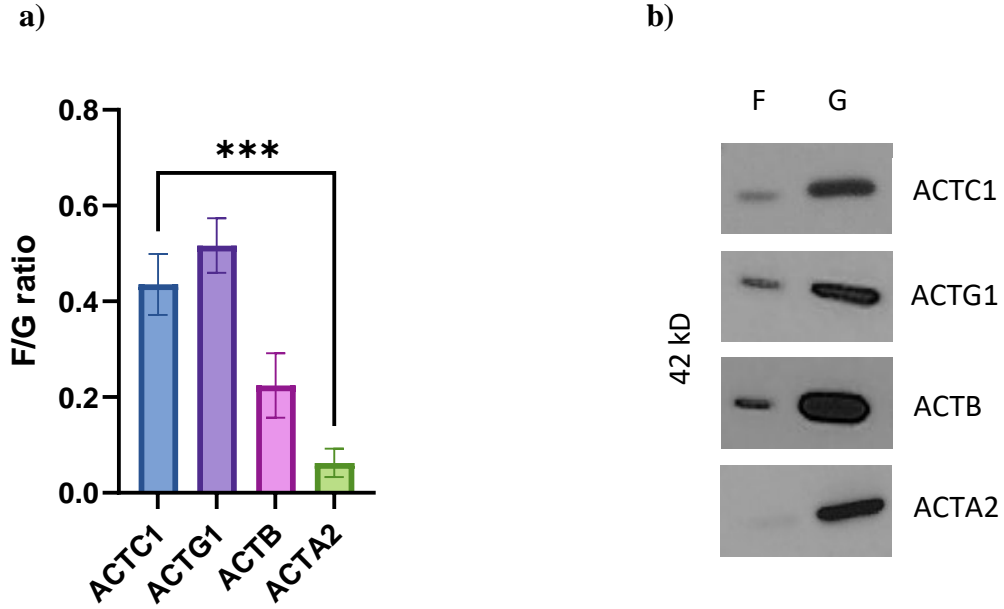


Figure 4. F/G ratios for ACTC1, ACTG1, ACTB and ACTA2 in UW426 SHH MB. a) F/G ratios for all 4 subunits in UW426. Graph represents mean of 3 biological replicates \pm SEM quantified by densitometry, $***P < .001$. **(b)** Western blot analysis of F- and G-fractions for UW426 probed for either ACTC1, ACTG1, ACTB or ACTA2. Equal volumes of F- and G-fractions were loaded.

1 **Aim (1.3) – Determination of actin subunit co-localization with F-actin**

2 Based on the previously described F/G ratios for each actin subunit in UW426, we sought to
3 determine whether these relationships could be recapitulated by immunofluorescence imaging. To
4 do so, we inspected the co-localization of each individual subunit (ACTC1, ACTG1, ACTB or
5 ACTA2) with F-actin (Phalloidin). Our results demonstrate a near complete co-localization of
6 ACTC1 (green) with F-actin (red) by merged images (**Figure 5**). This color overlap seen in
7 yellow/orange was observed across a minimum of 3 biological replicate Z-stack images (not shown
8 here). Although to a lesser extent, ACTG1 and ACTB were also shown to co-localize with F-actin.
9 However, their co-localization was greatly centered around the leading edge of UW426 cells where
10 lamellipodia and filipodia are known to originate. On the other hand, ACTA2 was almost entirely
11 deprived of co-localization with F-actin which is consistent with F/G ratio results.

12

13 **Aim (1.4) – Determination of ACTC1 co-localization with other actin subunits**

14 We sought to investigate ACTC1 co-localization with each of the other actin subunits (ACTG1,
15 ACTB and ACTA2) in UW426 to determine whether these results would have a similar co-
16 localization pattern. Not surprisingly, ACTC1 was found to co-localize with ACTG1 and ACTB
17 but not ACTA2 (**Figure 6**). This can be observed through the merged images where once again
18 ACTG1 and ACTB show bright yellow overlap, particularly at the leading edges, while ACTA2
19 cannot be seen to have any. These results were further validated by analysis of the Z-stack images
20 across at least 3 biological replicates.

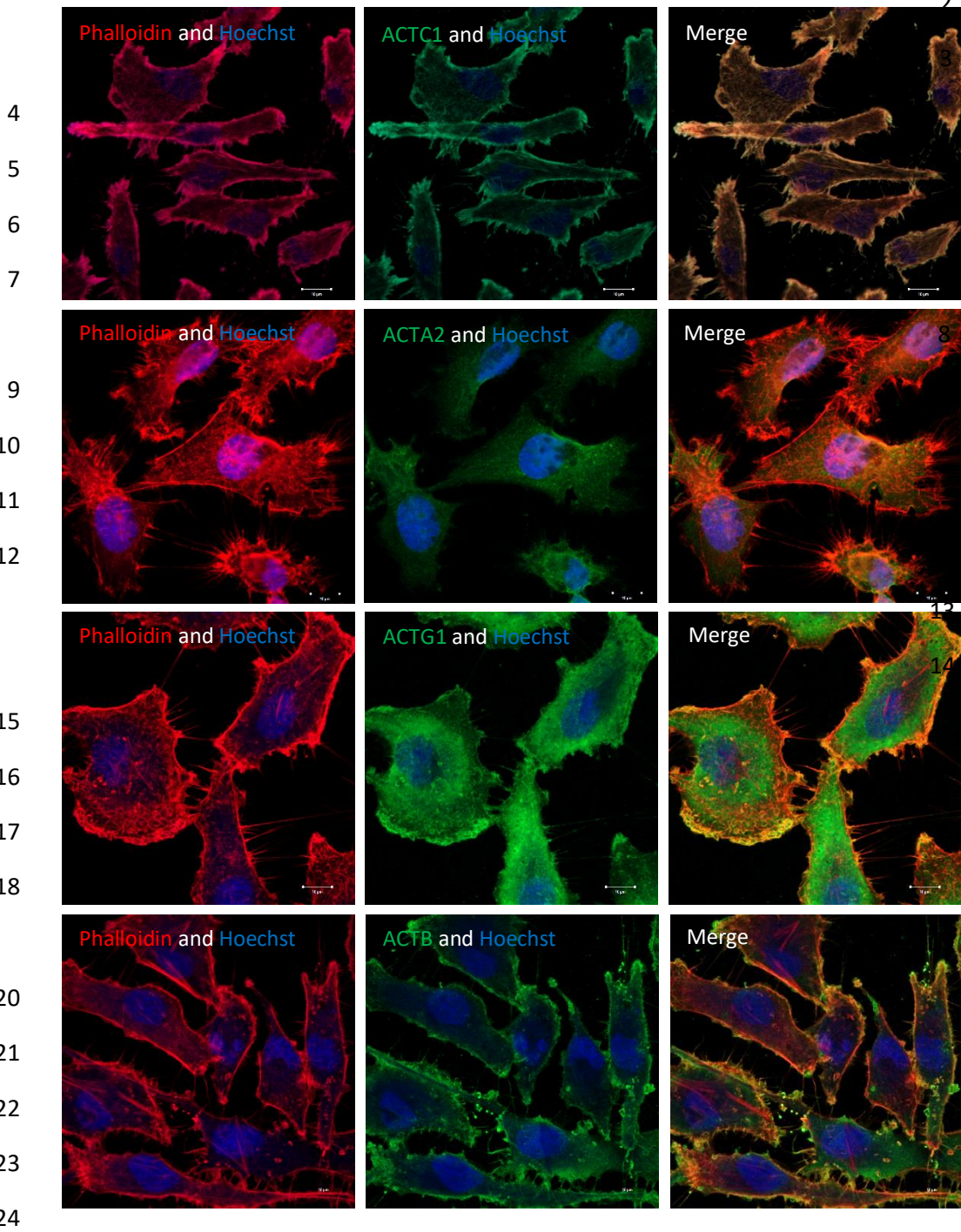
21

22

23

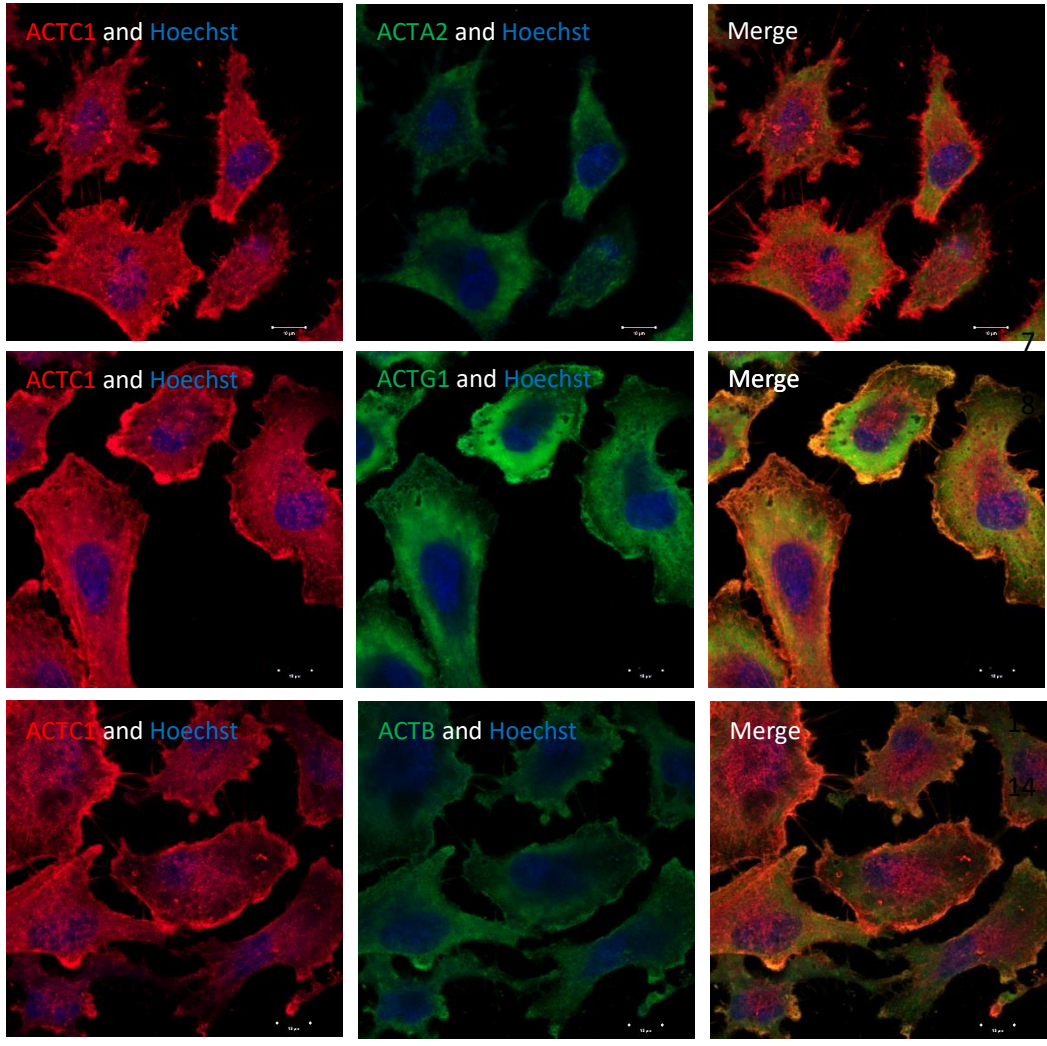
1

2



25 **Figure 5. Double-immunofluorescence imaging of ACTC1, ACTB, ACTG1 or ACTA2 with**
26 **Phalloidin.** Immunofluorescence imaging of UW426 cells labelled with phalloidin (F-Actin, red)
27 and anti-ACTC1, -ACTB, -ACTG1 or -ACTA2 antibody (green). Merged image shows the red-
28 green overlap as yellow/orange. Scale bar is 10 μ m.

1



4

5

6

9

10

11

12

15

16

17

18

19 **Figure 6. Double-immunofluorescence imaging of ACTB, ACTG1 or ACTA2 with ACTC1.**
20 Immunofluorescence imaging of UW426 cells labeled with ACTC1 (red) and anti-ACTB, -
21 ACTG1 or -ACTA2 antibody (green). Merged image shows the red-green overlap as yellow. Scale
22 bar is 10 μ m.

23

24

25

26

27

1 **Aim (1.5) – Determination of ACTC1 complex formation with individual actin subunits**

2 We sought to determine the possibility of complex formation of ACTC1 with either ACTG1 or
3 ACTB. Based on immunofluorescence imaging data, we predicted that co-localization between
4 these actin subunits could also translate into close physical proximity. To investigate this
5 hypothesis, we performed pulldown assays on UW426 or UW426-ACTC1-OE stable cell lines.
6 The UW426 ACTC1 OE line overexpresses ACTC1 conjugated to a FLAG tag. Pulling down
7 ACTC1 in wild-type UW426 using antibody-conjugated magnetic beads resulted in the pulldown
8 of both ACTG1 and ACTB as seen by Western blot analysis (**Figure 7a**). Furthermore, indirectly
9 pulling down ACTC1 by its FLAG tag in UW426-ACTC1-OE also resulted in pulldown of both
10 ACTG1 and ACTB (**Figure 7b**). The latter served as a secondary validation for the assay. These
11 results suggest complex formation between ACTC1, ACTG1 and ACTB.

12

13

14

15

16

17

18

19

20

21

22

23

1 **Aim 2 – To assess the effect of ACTC1 expression on stress fiber composition in SHH**
2 **medulloblastoma**

3 **Aim (2.1) – Quantification of stress fiber length distribution and total fiber length following**
4 **either ACTC1 KD or OE**

5 Stress fibers are contractile structures found in non-muscle cells that are composed of filamentous
6 actin (F-actin) bundles, α -actinin, and non-muscle myosin II⁶. Alterations in stress fiber
7 composition in a cell can be used to monitor changes in F-actin dynamics induced by drugs¹¹⁹. To
8 test if ACTC1 expression has an effect on F-actin dynamics, we measured the distributions of
9 stress fiber length in UW426 SHH cells with knockdown or overexpression of ACTC1 using an
10 automated stress fiber quantification software (**Supplementary Figure 13**). In UW426 cells which
11 show high levels of endogenous ACTC1 expression, no significant increase in fiber length was
12 observed when ACTC1 was overexpressed (**Figure 8a**). However, when ACTC1 was knocked
13 down, there was a decrease in the longer fiber lengths, with a shift in the dominating fibre length
14 from 6 to 3 μm ($P < .01$). Interestingly, there was an overall increase in total fiber length when
15 ACTC1 was knocked down, which is explained by an increase in the number of the shorter stress
16 fibers compared to the control ($P < .01$, **Figure 8b**). Thus, ACTC1 expression levels can modulate
17 the length of actin stress fibers in medulloblastoma.

18

19

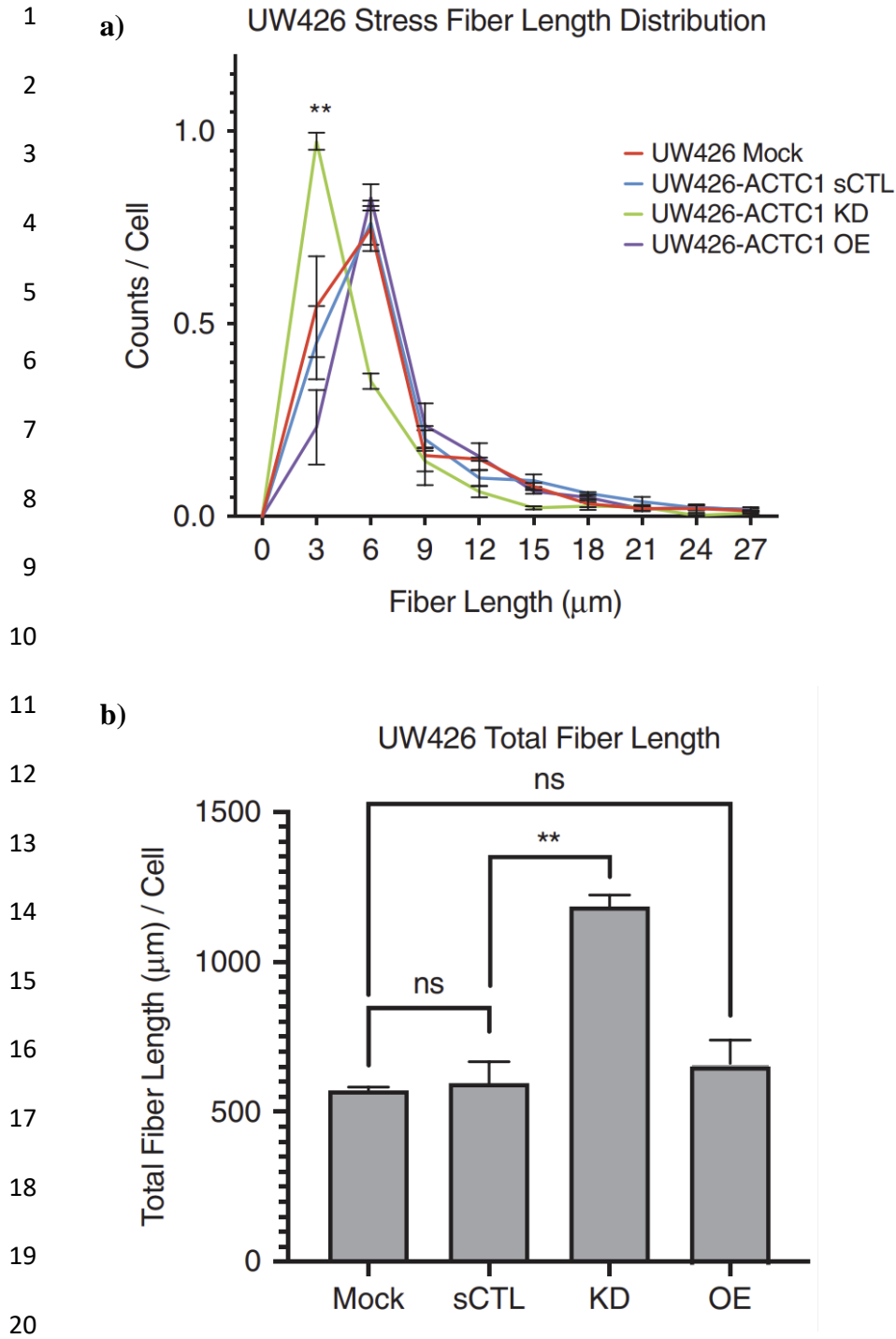
20

21

22

23

24



21 **Figure 8. Stress fiber length distribution and total fiber length following either ACTC1**
 22 **shRNA KD or stable OE. a)** Distribution of stress fiber lengths in wild-type (WT), ACTC1
 23 shRNA knockdown (ACTC1 KD), stable ACTC1 overexpressing (ACTC1 OE) UW426 cells.
 24 Counts were summed in bins of 3 μm. **b)** Total stress fiber length in wild-type (WT), ACTC1
 25 knockdown (ACTC1 KD), ACTC1 overexpressing (ACTC1 OE) UW426 cells. Graphs represent
 26 a mean of three biological replicates ± SEM. **P<0.01, ns - P>0.05.

1 **Aim 3 – To determine whether F/G ratios are maintained during mitotic inhibition in SHH**
2 **medulloblastoma resistant to apoptosis induced by Aurora kinase B inhibition.**

3 **Aim (3.1) – Quantification of SHH MB ACTC1 F/G ratio shifts following treatment with**
4 **the mitotic inhibitor AZD1152**

5 The high endogenous ACTC1 expression characteristic of SHH MB cells has been shown to
6 protect them against the toxic effects of mitotic inhibitor drugs⁷⁰. To better understand the
7 protection ACTC1 confers against this stress, we sought to investigate shifts in F-actin dynamics
8 in response to the mitotic inhibitor AZD1152. F- and G-actin fractions were analyzed by Western
9 blot analysis (**Figure 9a**). These results revealed that UW426 cells treated with AZD1152 for
10 either 24h or 48h did not have their ACTC1 F/G ratio undergo significant changes when compared
11 to DMSO or no treatment controls (**Figure 9b**). The no treatment control allowed to verify that
12 the DMSO concentration on its own was no cytotoxic as it did not significantly differ from the
13 F/G ratios for DMSO. The maintenance in F/G ratio in response to exposure to an Aurora kinase
14 B inhibitor further supports the idea that ACTC1 is a critical part of SHH MB F-actin. Furthermore,
15 maintenance of ACTC1 F-actin composition suggests that ACTC1 conveys this tumorigenic
16 phenotype mainly through its polymerized form.

17

18

19

20

21

22

23

24

1
2
3
4
5
6
7
8
9
10
11
12
13
14
15
16
17
18
19

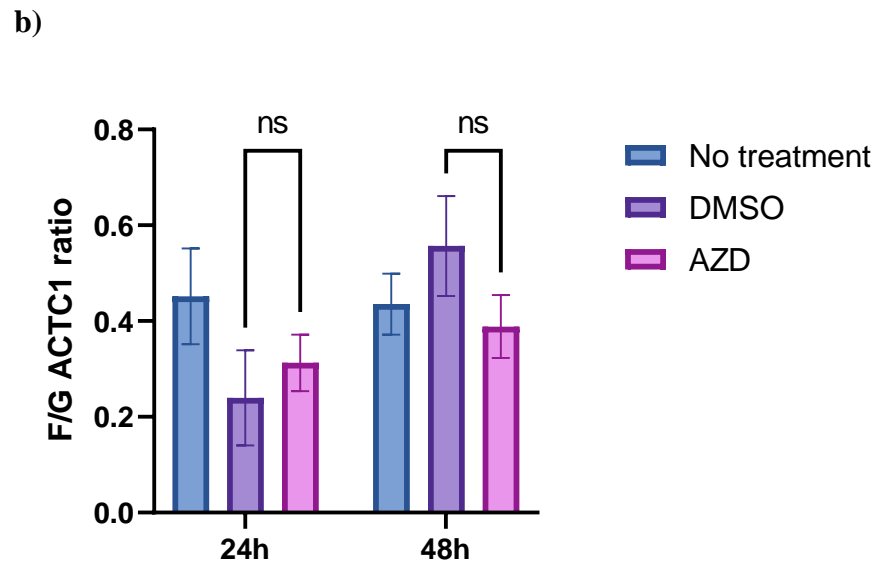
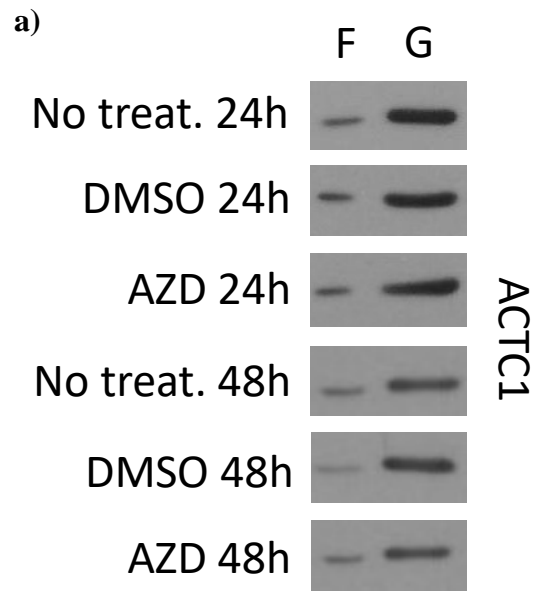


Figure 9. UW426 ACTC1 F/G ratio in response to Aurora kinase B inhibition at two different time points. a) Western blot analysis of UW426 cells exposed to 100 nM AZD1152, DMSO control or no treatment control (media) for 24h or 48h **b)** ACTC1 F/G ratios compiled from Western blot data. Graphs represent mean of 3 biological replicates \pm SEM. ******P < 0.01, ns - P > 0.05.

1 **Aim 4 – To assess the expression of ACTC1 in mice post-natal granule neuron progenitors.**

2 **Aim (4.1) – Determination of ACTC1 protein expression in early post-natal mouse**
3 **cerebellum**

4 Considering that SHH MB is mainly a pediatric tumour and originates in the cerebellum, we sought
5 to investigate whether ACTC1 is also expressed in early post-natal mouse cerebellum. ACTC1 is
6 not normally expressed in mature mammalian brain, but we hypothesized that it may be transiently
7 expressed at earlier time points to aid in key neurodevelopmental stages. Western blot analysis of
8 3 different post-natal day 1 mouse cerebellum lysates revealed strong ACTC1 expression (**Figure**
9 **10**). This suggests that ACTC1 expression has a role in normal early cerebellar development but
10 raises the question as to which cell type(s) it could be expressed in.

11

12

13

14

15

16

17

18

19

20

21

22

23

24

1
2
3
4
5
6
7
8
9
10
11
12
13
14
15
16
17
18
19
20
21

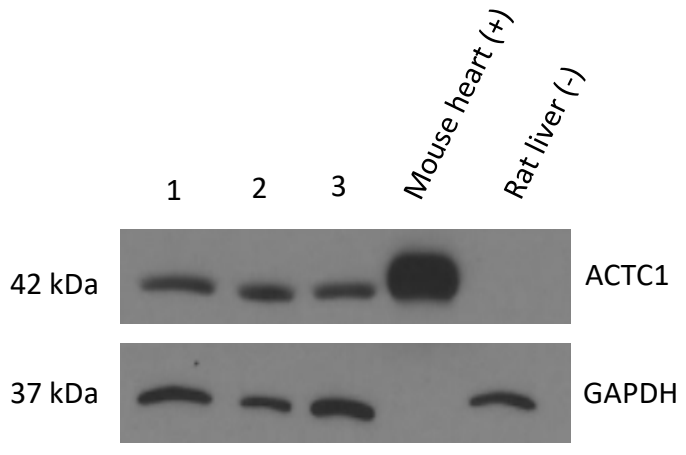


Figure 10. Western blot showing ACTC1 expression in post-natal day 1 mice whole cerebellum. Numbers 1-3 represent biological replicates of mouse cerebellum. Positive control (+) is mouse cardiac muscle lysate and negative control (-) is rat liver lysate. 10ug of protein was loaded in each lane except 1ug for the positive control. GAPDH is low in the positive control lane due to the lower amount of protein loaded.

1 **Aim (4.2) – Determination of ACTC1 protein expression in GNPs**

2 Following the discovery of ACTC1 expression in early post-natal mouse cerebellum, we sought
3 to investigate its source on the cellular level. The cell type of origin of SHH MB is strongly
4 suggested to be the granule cell progenitor¹²⁰. Therefore, we performed isolation of granule neuron
5 progenitor cells from early post-natal mouse cerebellum to determine whether aberrant ACTC1
6 expression in SHH MB could be recapitulating a neurodevelopmental phenotype characteristic of
7 GNPs. We found ACTC1 to be strongly expressed across all 3 biological replicates ranging from
8 day 3 to day 8 post-natal mouse GNPs (**Figure 11**). These results suggest that the ACTC1
9 expression observed in post-natal day 1 mouse cerebellum (**Figure 10**) is likely coming from
10 GNPs considering their high abundance in early mouse cerebellum. However, further experiments
11 remain to be done to assess its expression in other cell types such as astrocytes and
12 oligodendrocytes.

13
14
15
16
17
18
19
20
21
22
23

1
2
3
4
5
6
7
8
9
10
11
12
13
14
15
16
17
18
19
20
21
22
23
24
25
26

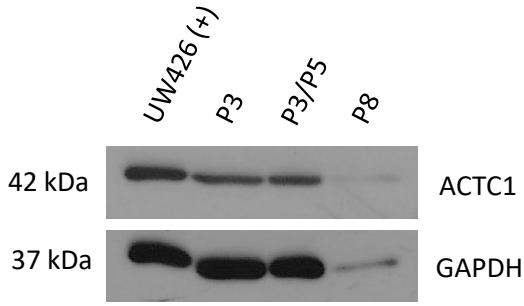


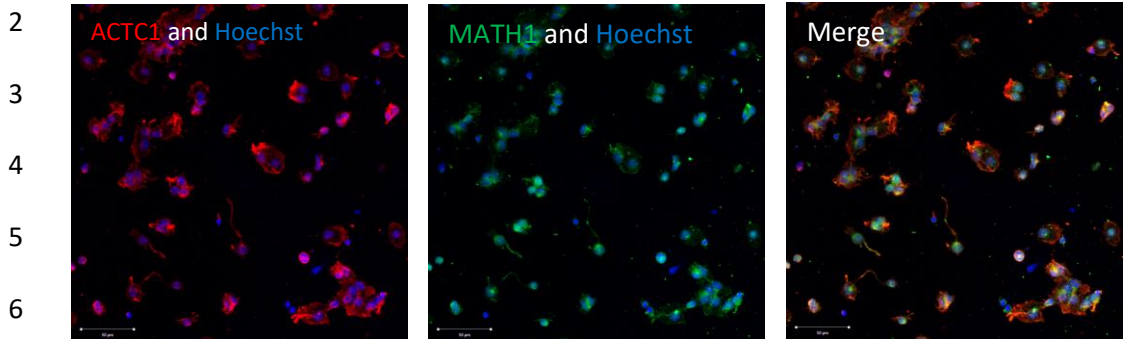
Figure 11. Western blot analysis of ACTC1 expression in mouse granule neuron and progenitor cells. The P3 and P8 lanes represents mouse cerebellum from post-natal day 3 and day 8 mice, respectively. The P3/P5 lane represents an equal mixture of post-natal day 3 and 5 mouse cerebellum. Positive control (+) is UW426. 10ug of protein was loaded per well.

1 **Aim (4.3) – Quantification of granule neuron progenitor extraction purity from mouse**
2 **cerebellum**

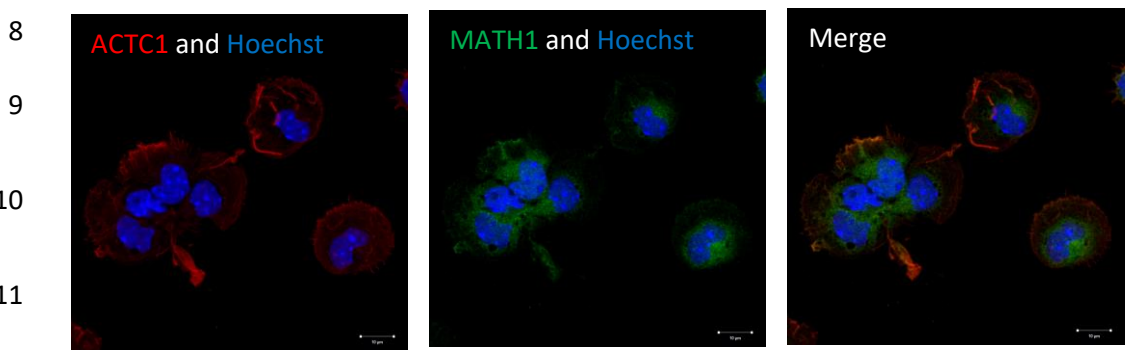
3 The granule neuron/progenitor extraction from early post-natal mouse cerebellum protocol is a
4 technically challenging procedure to follow. Granule neuron progenitor purity can vary greatly
5 depending on the mouse cerebellum collection timepoint and extraction efficiency. To validate
6 that ACTC1 protein quantification by Western blot analysis was a faithful representation of GNP
7 expression, we sought to measure GNP purity by immunofluorescence imaging for the P3 and P5
8 mouse cerebellum samples (**Figure 12a, b**). Results demonstrated that 94.42% of cells stained
9 with Hoechst nuclear stain were also MATH-1 positive, a GNP-specific cell marker (**Figure 12c**).
10 Additionally, immunofluorescence imaging allowed us to determine that 93.58% of cells were also
11 ACTC1 positive (**Figure 12c**). This translates into a non-significant difference versus the
12 percentage of MATH-1 positive cells indicating with high certainty that GNP cells express
13 ACTC1.

14
15
16
17
18
19
20
21
22
23
24

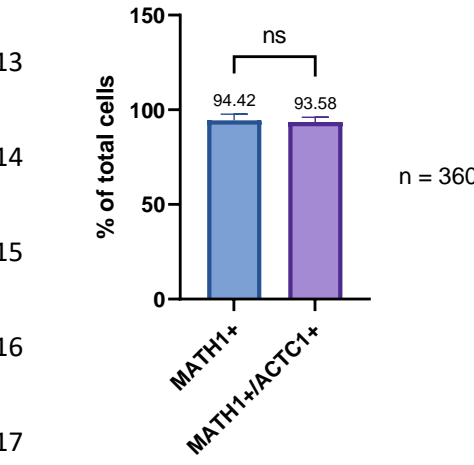
1 a)



7 b)



12 c)



18 **Figure 12. Co-immunofluorescence imaging of ACTC1 expression in granule neuron**
19 **progenitor cells.** Immunofluorescence imaging of P3/P5 GNP cells labeled with ACTC1 (red)
20 and MATH-1 antibody (green) at a) 200X magnification (scale bar is 50 μm) and b) 630X
21 magnification (scale bar is 20 μm). Merged image shows MATH-1 positive cells also expressing
22 ACTC1. c) Statistical analysis of the percentage of cells either MATH-1 or MATH-1/ACTC1
23 positive. A total of 360 cells were analyzed.

24

1 **Discussion**

2

3 **ACTC1 co-localizes and forms complexes with both non-muscle actin isoforms in F-actin**

4 In this study, we describe the sub-cellular localization and polymerization of ACTC1 with other
5 actin subunits in SHH MB. Dysregulation of normal actin dynamics has been long known to be
6 involved in tumorigenesis, especially in cancer cell migration and invasion⁵⁶. A handful of studies
7 have recently found aberrant ACTC1 expression in both MB and GBM, but the mechanism by
8 which it confers resistance to apoptosis and enables increased cell migration and survival is still
9 unknown^{68,70}. Since ACTC1 is normally only found in heart tissue of mature mammals, it becomes
10 an interesting therapeutic target for detecting and treating CNS tumours. It also raises the question
11 as to how these cells manage to leverage its expression on a sub-cellular level.

12

13 Our finding that various actin subunits are expressed in SHH MB cells is concordant with the
14 finding of subunit mRNA expression in bulk SHH MB tumours as assessed by our collaborator
15 Dr. Marc Remke in the Cavalli/Remke dataset (**Figure 1**). These results suggest the presence of a
16 broad range of actin subunits that could be interacting with ACTC1 in SHH MB. Further
17 comparison with the recently published single-cell RNA sequencing MB tumour dataset would
18 provide for additional validation of these relationships¹²¹. F/G ratios were measured for each of
19 these subunits and portrayed in our immunofluorescence imaging results (**Figure 5, 6**). Elevated
20 F/G ratios for ACTC1, ACTG1 and ACTB corresponded to strong co-localization with F-actin
21 while a significantly lower F/G ratio for ACTA2 resulted in strong association to the globular form
22 and lack of F-actin and ACTC1 co-localization. These findings suggest that although other muscle
23 actin isoforms exhibit overexpression in SHH MB, they may not be important in directly regulating

1 ACTC1 dynamics. On the other hand, strong co-localization of ACTC1 with ACTG1 and ACTB
2 in F-actin at the leading edge suggests that they contribute to ACTC1 filament stability. Validation
3 of complex formation between ACTC1 and ACTG1/ACTB further strengthens this assumption.
4 Given that the leading edge is the sub-cellular region where lamellipodia and filipodia form, it is
5 possible that non-muscle isoforms are preferentially recruited at these regions to enhance SHH
6 MB migratory ability and invasiveness⁵¹. Furthermore, studies have shown that both ACTG1 and
7 ACTB expression are essential for neuronal differentiation and plasticity¹²². ACTG1 is known to
8 have a relatively constant expression throughout brain development while ACTB expression
9 rapidly decreases with age¹²². This could possibly explain their strong relationship with ACTC1
10 in SHH MB F-actin. Expression of all three of these actin isoforms in F-actin may simply be
11 recapitulating normal granule cell progenitor actin structural diversity. Further work is needed to
12 determine the importance of non-muscle actin subunits in the maintenance of ACTC1 in its
13 polymerized form, and subsequent impacts on SHH MB phenotypes.

14

15 **ACTC1 expression levels modify stress fiber composition in SHH cells**

16 In this study, we have demonstrated that alteration in ACTC1 levels in medulloblastoma cells has
17 a direct effect on stress fiber formation. Knockdown of ACTC1 in SHH cells results in a shift
18 toward shorter stress fibers, coupled with an increase total fiber formation. This would suggest that
19 ACTC1 is critical to stress fiber stability and its KD leads to a greater number of short fibers due
20 to stress fiber breakdown. Additionally, we suggest that the overall increase in total fiber length
21 could be driven by the cell need to compensate for this shift. Many key cytoskeletal functions rely
22 on long stress fibers and therefore an increase in total fiber formation would allow the SHH MB
23 cell to maximize its structural integrity despite losing some flexibility in the tasks it can

1 accomplish²⁶. Further experiments measuring the polymerization properties and actin binding
2 protein interactions of ACTC1 F-actin, as well as those of co-polymers with ACTG1 and ACTB
3 subunits will help to define the cytoskeletal changes that occur when ACTC1 is expressed.

4

5 **Maintenance of ACTC1 in F-actin is a defining feature of mitotic inhibitor resistance by** 6 **SHH MB**

7 In this study, we tested the impact of Aurora kinase B inhibition on UW426 ACTC1
8 polymerization dynamics. AURKB inhibitors are small molecules capable of disrupting normal
9 cell cycle progression⁹⁹. The role of AURKB is still not completely understood but reports have
10 pointed to its importance in regulating chromosome condensation and segregation as well as for
11 cleavage furrow formation and cytokinesis⁹⁹. SHH MB, which aberrantly expresses ACTC1, is
12 known to resist treatment with the mitotic inhibitor AZD1152 while Group 3 MB expressing very
13 low endogenous ACTC1 levels undergoes significant cell death⁷⁰. Interestingly, F/G ratios
14 remained stable upon mitotic inhibitor treatment at both 24h and 48h. We suspect that UW426
15 cells may be promoting ACTC1 polymerization stability upon mitotic inhibitor treatment. This
16 would suggest that ACTC1 protects SHH MB cells against mitotic stress through enhanced F-actin
17 integrity. Considering the importance of F-actin in the formation of the cleavage ring in
18 cytokinesis, ACTC1 could be protecting against AURKB inhibition by increasing ring stability
19 and thus, allowing for completion of cell division¹²³. Breakdown of F-actin is also known to lead
20 to apoptosis signaling which further validates these results⁵³. To further evaluate whether ACTC1
21 exerts its functional roles through its filamentous form, we plan to individually overexpress two
22 different ACTC1 non-polymerizing mutant plasmids (G247D- & Y116C-ACTC1) in SHH MB
23 cells. The overexpression of these mutants is hypothesized to cause instability in F-actin and a
24 decrease in mean fiber length within the cell. These mutations will allow us to test if disruption of

1 F-actin stability results in negative effects on SHH MB cell viability and migration ability. This
2 next set of experiments will be key to determining whether ACTC1 exerts its tumorigenic benefits
3 mainly through its filamentous form as these previous assays suggest.

4

5 **ACTC1 is expressed in mouse granule neuron progenitor cells**

6 Finally, we sought to investigate the neurodevelopmental implications of ACTC1 in mouse post-
7 natal granule progenitor cells. Given that ACTC1 is not normally expressed in the adult brain, we
8 hypothesised that it may be recapitulating an early neurodevelopmental phenotype. Multiple
9 studies have suggested the granule neuron progenitor cell as being the cell of origin for SHH
10 MB^{86,87}. We successfully demonstrated for the first time that early-post natal mouse cerebellum
11 strongly express ACTC1 protein. Isolation of granule neuron progenitors with high purity further
12 demonstrated ACTC1 expression by both Western blot and immunofluorescence microscopy.
13 These results suggest that ACTC1 expression in SHH MB is likely recapitulating an early
14 neurodevelopmental phenotype rather than being an aberrant gene activation downstream of an
15 oncogenic effector. Additionally, expression of ACTC1 in early neurodevelopment could provide
16 insight into the vast array of genetic neurodevelopmental disorders such as 22q11.2DS and
17 CHARGE syndrome which have also been associated with congenital heart defects^{112,113}. A large-
18 scale transcriptome analysis could help determine whether abnormal ACTC1 expression at an
19 early stage could be causing some of these cardiac issues.

20

21 To further investigate the neurodevelopmental relationship between ACTC1, granule neuron
22 progenitors and SHH MB, it will be important to look at different parts of the Shh pathway which
23 have control over downstream actin cytoskeleton dynamics. For example, inhibition of some key

1 regulatory proteins in the Shh pathway such as Gli1 are likely to impact actin subunit diversity and
2 offer new avenues for therapeutic treatment. Alternatively, the availability of newly published
3 datasets will allow us to study the actin subunit expression from MB tumour specific RNAseq
4 datasets in relationship to mutations resulting in Shh pathway activation¹²¹. It will of particular
5 interest to determine whether ACTC1 overexpression is linked to any Shh pathway mutations.
6 Furthermore, we'd like to test whether Shh depletion in GNP culture influences ACTC1 protein
7 expression levels. This will determine if there is a concrete relationship between Shh signaling and
8 ACTC1 expression. Finally, testing the role of ACTC1 in GNP migration and survival through
9 knockdown assays will allow us to compare the functional similarities with SHH MB.

10

11 This study is subject to certain limitations. First of all, tissue-specific actin isoform antibodies used
12 for Western blots and immunofluorescence imaging were validated with both positive and negative
13 controls for specificity. However, non-tissue specific isoform antibodies could not be tested with
14 a negative control due to their ubiquitous expression in mammals cells. A CRISPR knockout
15 (KO) experiment would need to be done to generate ACTG1 and ACTB KO HEK293 cell lines
16 that can be used for lysate controls. Second of all, the F/G -actin assay relies on an F-actin
17 stabilizing buffer while lysing the cells. As F-actin spontaneously disassembles into G-actin, it is
18 expected that the buffer will not be able to prevent degradation of all F-actin strands. Therefore,
19 G-actin fractions are expected to result in slightly stronger bands on Western blots. This assay
20 should therefore be exclusively used to evaluate F/G ratios between conditions as the error should
21 be consistent across samples. Third of all, it is important to note that co-immunoprecipitation
22 assays can only provide information regarding protein-protein interactions in complex. These
23 assays do not enable us to evaluate the co-polymerization potential of different actin subunits. To

1 determine co-polymerization, tightly controlled actin dynamics assays would need to be performed
2 using purified subunit samples. Finally, the limited availability of early-post natal mice has
3 reduced our ability to collect granule cell progenitor biological replicates from identical time
4 points. We aim to pursue further collection experiments for this reason as well as leverage the
5 accessibility of different collection time points to investigate whether ACTC1 expression is
6 temporally regulated.

7

8

9

10

11

12

13

14

15

16

17

18

19

20

21

22

1 **Conclusion**

2 This study is the first to demonstrate ACTC1 co-localization and complex formation with both
3 non-muscle actin isoforms (ACTB and ACTG1) in SHH MB F-actin. Additionally, ACTC1 was
4 also shown to be a major constituent of F-actin. Co-localization was shown to be highly centered
5 around the cell leading edge suggesting importance for filipodia and lamellipodia formation.
6 ACTA2 did not co-localize with neither ACTC1 nor F-actin suggesting other muscle actin
7 isoforms may not play an important role in ACTC1 dynamics. Although we did not investigate the
8 interactions of ACTC1 with the remaining two actin isoforms (ACTG2 and ACTA1), this study
9 represents an important first step in establishing the mechanism of action of ACTC1 in SHH MB.

10

11 This study is the first to demonstrate ACTC1 importance in modulating stress fiber composition.
12 Knockdown of ACTC1 induced a shift towards a shorter stress fiber distribution and increased
13 overall stress fiber formation, suggesting the importance of ACTC1 in maintaining F-actin
14 stability. Alternatively, overexpression of ACTC1 did not induce any significant change on stress
15 fiber composition. Further work is needed to assess the role of non-muscle actin subunits in
16 maintaining this fiber integrity and whether functional characteristics provided by ACTC1
17 overexpression are dependent of its integration into the F-actin.

18

19 This study is the first to demonstrate that maintenance of ACTC1 composition in F-actin is a
20 defining feature of mitotic inhibitor resistance by SHH MB. ACTC1 F/G ratios were not
21 significantly altered following treatment with an AURKB inhibitor which suggests that ACTC1
22 protects SHH MB cells against mitotic stress through enhanced F-actin integrity. Further work is

1 needed to assess whether non-muscle actin isoform as well as total actin F/G ratios are equally
2 maintained.

3

4 This study was the first to demonstrate the expression of ACTC1 in early post-natal mouse
5 cerebellum and granule neuron progenitor cells. GNPs express ACTC1 at a near 100% frequency
6 which suggests that ACTC1 expression in SHH MB is likely recapitulating an early
7 neurodevelopmental phenotype. Further work is needed to assess whether ACTC1 expression is
8 dependent upon Shh signaling.

9

10 Overall, this study was successful in demonstrating the importance of actin subunit diversity in
11 SHH MB migration and survival and elucidating the neurodevelopmental origin of aberrant
12 ACTC1 expression found in SHH MB.

13

14

15

16

17

18

19

20

21

22

23

1 **APPENDIX 1. SUPPLEMENTARY INFORMATION**

2

3 **Table 2: Western blot antibody list.**

Primary antibody	Concentration	Secondary antibody	Concentration
Rabbit anti-ACTC1 (Abcam; ab218549)	1:1000	Goat anti-rabbit HRP-linked (Cell Signaling; 7074)	1:30,000
Mouse anti-ACTB (Sigma; MABT825)	1:2000	Goat anti-mouse HRP-linked (Cell Signaling; 7076)	1:10,000
Mouse anti-ACTG1 (Sigma; MABT824)	1:1000	Goat anti-mouse HRP-linked (Cell Signaling; 7076)	1:30,000
Mouse anti-ACTA2 (Sigma; A2547)	1:1000	Goat anti-mouse HRP-linked (Cell Signaling; 7076)	1:5000
Rabbit anti-GAPDH (14C10) (Cell Signaling; 2118)	1:1000	Goat anti-rabbit HRP-linked (Cell Signaling; 7074)	1:30,000
Mouse ANTI-FLAG M2 (Sigma, F1804)	1:1000	Goat anti-mouse HRP-linked (Cell Signaling; 7076)	1:30,000

4

5

6

7

1 **Table 3: Immunofluorescence antibody list.**

2

Primary antibody	Concentration	Secondary antibody	Concentration
Rabbit anti-ACTC1 (Abcam; ab218549)	1:1000	Goat anti-rabbit, 488 (Thermo; A11034)	1:500
Mouse anti-ACTB (Sigma; MABT825)	1:200	Goat anti-mouse, 594 (Thermo; A11032) or Goat anti-mouse, 488 (Thermo; A21202)	1:500
Mouse anti-ACTG1 (Sigma; MABT824)	1:200	Goat anti-mouse, 594 (Thermo; A11032) or Goat anti-mouse, 488 (Thermo; A21202)	1:500
Mouse anti-ACTA2 (Sigma; A2547)	1:500	Goat anti-mouse, 594 (Thermo; A11032) or Goat anti-mouse, 488 (Thermo; A21202)	1:500
Mouse ANTI-FLAG M2 (Sigma, F1804)	1:500	Goat anti-mouse, 594 (Thermo; A11032) or Goat anti-mouse, 488 (Thermo; A21202)	1:1000
Rabbit anti-MATH1 (ATO1) (Thermo, 21215-1-AP)	1:500	Goat anti-rabbit, 488 (Thermo; A11034)	1:500
Mouse ANTI-FLAG M2 (Sigma, F1804)	1:500	Goat anti-mouse, 594 (Thermo; A11032) or Goat anti-mouse, 488 (Thermo; A21202)	1:500
Mouse anti-myelin CNPase (Biolegen; clone SMI 91)	1:500	Goat anti-mouse, 594 (Thermo; A11032) or Goat anti-mouse, 488 (Thermo; A21202)	1:500
Alexa Fluor 594 anti- GFAP (Biolegend; clone SMI 25)	1:500	N/A	N/A

Alexa-Fluor 647 Phalloidin (Thermo; A22287)	1:20	N/A	N/A
Hoechst 33342 (Thermo; H1399)	1:4000	N/A	N/A

1

2

3

4

5

6

7

8

9

10

11

12

13

14

15

1 **Table 4: Parameter settings used for stress fiber analysis using the FSegment software.**

2

Parameter Presetting	
Min expected Filament Width	4 Pixel
Max expected Filament Width	18 Pixel
Parameter Finetuning	
Gaussian Sigma	3.5 Pixel
Directional Top-Hat	18 Pixel
Path Opening	23 Pixel
Hysteresis Thresh. Min Area	440 Pixel ²
Step Length	16 Pixel
Maximal Curvature	22 */Step Length
Max Distance	4 *Step Length
Maximal Kingking	25 *
Min. Filament Length	3 *Step Length

3

4

5

6

7

8

9

10

11

12

13

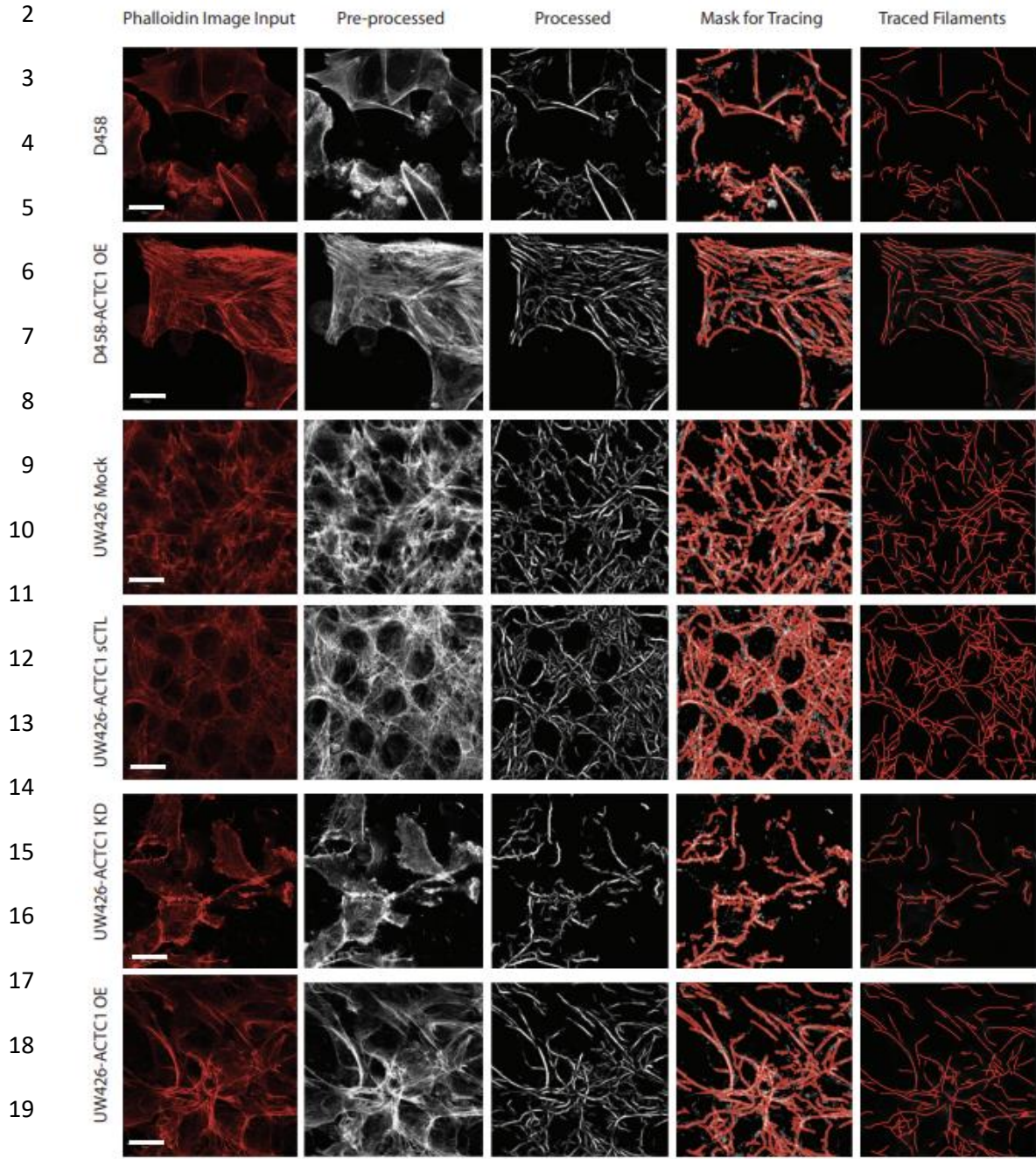
14

15

16

17

1 **Figure 13. Image processing for stress fiber quantification.**



1 Bibliography

- 2 1. Lambrechts, A., Van Troys, M. & Ampe, C. The actin cytoskeleton in normal and pathological cell
3 motility. *Int. J. Biochem. Cell Biol.* **36**, 1890–1909 (2004).
- 4 2. Ridley, A. J. Rho GTPases and actin dynamics in membrane protrusions and vesicle trafficking.
5 *Trends Cell Biol.* **16**, 522–529 (2006).
- 6 3. Kristó, I., Bajusz, I., Bajusz, C., Borkúti, P. & Vilmos, P. Actin, actin-binding proteins, and actin-related
7 proteins in the nucleus. *Histochem. Cell Biol.* **145**, 373–388 (2016).
- 8 4. Erba, H. P., Gunning, P. & Kedes, L. Nucleotide sequence of the human γ cytoskeletal actin mRNA:
9 anomalous evolution of vertebrate non-muscle actin genes. *Nucleic Acids Res.* **14**, 5275–5294
10 (1986).
- 11 5. Dominguez, R. & Holmes, K. C. Actin Structure and Function. *Annu. Rev. Biophys.* **40**, 169–186
12 (2011).
- 13 6. Perrin, B. J. & Ervasti, J. M. The actin gene family: function follows isoform. *Cytoskelet. Hoboken NJ*
14 **67**, 630–634 (2010).
- 15 7. Varland, S., Vandekerckhove, J. & Drazic, A. Actin Post-translational Modifications: The Cinderella of
16 Cytoskeletal Control. *Trends Biochem. Sci.* **44**, 502–516 (2019).
- 17 8. Lin, J. & Redies, C. Histological evidence: housekeeping genes beta-actin and GAPDH are of limited
18 value for normalization of gene expression. *Dev. Genes Evol.* **222**, 369–376 (2012).
- 19 9. Bas, A., Forsberg, G., Hammarström, S. & Hammarström, M.-L. Utility of the housekeeping genes
20 18S rRNA, beta-actin and glyceraldehyde-3-phosphate-dehydrogenase for normalization in real-time
21 quantitative reverse transcriptase-polymerase chain reaction analysis of gene expression in human
22 T lymphocytes. *Scand. J. Immunol.* **59**, 566–573 (2004).
- 23 10. Bunnell, T. M. & Ervasti, J. M. Delayed embryonic development and impaired cell growth and
24 survival in Actg1 null mice. *Cytoskelet. Hoboken NJ* **67**, 564–572 (2010).

- 1 11. Erba, H. P., Eddy, R., Shows, T., Kedes, L. & Gunning, P. Structure, chromosome location, and
2 expression of the human gamma-actin gene: differential evolution, location, and expression of the
3 cytoskeletal beta- and gamma-actin genes. *Mol. Cell. Biol.* **8**, 1775–1789 (1988).
- 4 12. Matera, I. *et al.* Variants of the ACTG2 gene correlate with degree of severity and presence of
5 megacystis in chronic intestinal pseudo-obstruction. *Eur. J. Hum. Genet.* **24**, 1211–1215 (2016).
- 6 13. Maluleke, T., Mangray, H., Arnold, M., Moore, H. A. & Moore, S. W. Recurrent ACTG2 gene variation
7 in African degenerative visceral leiomyopathy. *Pediatr. Surg. Int.* **35**, 439–442 (2019).
- 8 14. Halim, D. *et al.* ACTG2 variants impair actin polymerization in sporadic Megacystis Microcolon
9 Intestinal Hypoperistalsis Syndrome. *Hum. Mol. Genet.* **25**, 571–583 (2016).
- 10 15. Frank, D. *et al.* Cardiac α -Actin (ACTC1) Gene Mutation Causes Atrial-Septal Defects Associated With
11 Late-Onset Dilated Cardiomyopathy. *Circ. Genomic Precis. Med.* **12**, e002491 (2019).
- 12 16. Sparrow, J. C. *et al.* Muscle disease caused by mutations in the skeletal muscle alpha-actin gene
13 (ACTA1). *Neuromuscul. Disord. NMD* **13**, 519–531 (2003).
- 14 17. North, K. N. & Laing, N. G. Skeletal muscle alpha-actin diseases. *Adv. Exp. Med. Biol.* **642**, 15–27
15 (2008).
- 16 18. Yuan, S.-M. α -Smooth Muscle Actin and ACTA2 Gene Expressions in Vasculopathies. *Braz. J.*
17 *Cardiovasc. Surg.* **30**, 644–649 (2015).
- 18 19. Burger, J. *et al.* Molecular phenotyping and functional assessment of smooth muscle-like cells with
19 pathogenic variants in aneurysm genes ACTA2, MYH11, SMAD3 and FBN1. *Hum. Mol. Genet.* **30**,
20 2286–2299 (2021).
- 21 20. Muller, J. *et al.* Sequence and comparative genomic analysis of actin-related proteins. *Mol. Biol. Cell*
22 **16**, 5736–5748 (2005).
- 23 21. dos Remedios, C. G. *et al.* Actin binding proteins: regulation of cytoskeletal microfilaments. *Physiol.*
24 *Rev.* **83**, 433–473 (2003).

- 1 22. Courtemanche, N. Mechanisms of formin-mediated actin assembly and dynamics. *Biophys. Rev.* **10**,
2 1553–1569 (2018).
- 3 23. Edwards, M. *et al.* Capping protein regulators fine-tune actin assembly dynamics. *Nat. Rev. Mol. Cell*
4 *Biol.* **15**, 677–689 (2014).
- 5 24. Harms, C. *et al.* Neuronal gelsolin prevents apoptosis by enhancing actin depolymerization. *Mol.*
6 *Cell. Neurosci.* **25**, 69–82 (2004).
- 7 25. Liu, T. *et al.* Cofilin-mediated Neuronal Apoptosis via p53 Translocation and PLD1 Regulation. *Sci.*
8 *Rep.* **7**, 11532 (2017).
- 9 26. Ndozangue-Touriguine, O., Hamelin, J. & Bréard, J. Cytoskeleton and apoptosis. *Biochem.*
10 *Pharmacol.* **76**, 11–18 (2008).
- 11 27. Segundo, C. *et al.* Surface molecule loss and bleb formation by human germinal center B cells
12 undergoing apoptosis: role of apoptotic blebs in monocyte chemotaxis. *Blood* **94**, 1012–1020
13 (1999).
- 14 28. Desouza, M., Gunning, P. W. & Stehn, J. R. The actin cytoskeleton as a sensor and mediator of
15 apoptosis. *Bioarchitecture* **2**, 75–87 (2012).
- 16 29. Franklin-Tong, V. E. & Gourlay, C. W. A role for actin in regulating apoptosis/programmed cell death:
17 evidence spanning yeast, plants and animals. *Biochem. J.* **413**, 389–404 (2008).
- 18 30. Blanchoin, L., Boujemaa-Paterski, R., Sykes, C. & Plastino, J. Actin Dynamics, Architecture, and
19 Mechanics in Cell Motility. *Physiol. Rev.* **94**, 235–263 (2014).
- 20 31. Weinberg, J. & Drubin, D. G. Clathrin-mediated endocytosis in budding yeast. *Trends Cell Biol.* **22**, 1–
21 13 (2012).
- 22 32. Yi, K. & Li, R. Actin cytoskeleton in cell polarity and asymmetric division during mouse oocyte
23 maturation. *Cytoskelet. Hoboken NJ* **69**, 727–737 (2012).

- 1 33. Yang, C. & Svitkina, T. Filopodia initiation: focus on the Arp2/3 complex and formins. *Cell Adhes.*
2 *Migr.* **5**, 402–408 (2011).
- 3 34. Barral, J. & Martin, P. The physical basis of active mechanosensitivity by the hair-cell bundle. *Curr.*
4 *Opin. Otolaryngol. Head Neck Surg.* **19**, 369–375 (2011).
- 5 35. Revenu, C., Athman, R., Robine, S. & Louvard, D. The co-workers of actin filaments: from cell
6 structures to signals. *Nat. Rev. Mol. Cell Biol.* **5**, 635–646 (2004).
- 7 36. Lee, S. & Kumar, S. Actomyosin stress fiber mechanosensing in 2D and 3D. *F1000Research* **5**, F1000
8 Faculty Rev-2261 (2016).
- 9 37. Hotulainen, P. & Lappalainen, P. Stress fibers are generated by two distinct actin assembly
10 mechanisms in motile cells. *J. Cell Biol.* **173**, 383–394 (2006).
- 11 38. Gupton, S. L. & Waterman-Storer, C. M. Spatiotemporal feedback between actomyosin and focal-
12 adhesion systems optimizes rapid cell migration. *Cell* **125**, 1361–1374 (2006).
- 13 39. Bunnell, T. M., Burbach, B. J., Shimizu, Y. & Ervasti, J. M. β -Actin specifically controls cell growth,
14 migration, and the G-actin pool. *Mol. Biol. Cell* **22**, 4047–4058 (2011).
- 15 40. Crawford, K. *et al.* Mice lacking skeletal muscle actin show reduced muscle strength and growth
16 deficits and die during the neonatal period. *Mol. Cell. Biol.* **22**, 5887–5896 (2002).
- 17 41. Kumar, A. *et al.* Rescue of cardiac alpha-actin-deficient mice by enteric smooth muscle gamma-
18 actin. *Proc. Natl. Acad. Sci. U. S. A.* **94**, 4406–4411 (1997).
- 19 42. Schildmeyer, L. A. *et al.* Impaired vascular contractility and blood pressure homeostasis in the
20 smooth muscle alpha-actin null mouse. *FASEB J. Off. Publ. Fed. Am. Soc. Exp. Biol.* **14**, 2213–2220
21 (2000).
- 22 43. Tondeleir, D. *et al.* Cells lacking β -actin are genetically reprogrammed and maintain conditional
23 migratory capacity. *Mol. Cell. Proteomics MCP* **11**, 255–271 (2012).

- 1 44. Kaech, S., Fischer, M., Doll, T. & Matus, A. Isoform Specificity in the Relationship of Actin to
2 Dendritic Spines. *J. Neurosci.* **17**, 9565–9572 (1997).
- 3 45. Mounier, N., Perriard, J. C., Gabbiani, G. & Chaponnier, C. Transfected muscle and non-muscle actins
4 are differentially sorted by cultured smooth muscle and non-muscle cells. *J. Cell Sci.* **110 (Pt 7)**,
5 839–846 (1997).
- 6 46. Kashina, A. S. Regulation of actin isoforms in cellular and developmental processes. *Semin. Cell Dev.*
7 *Biol.* **102**, 113–121 (2020).
- 8 47. Buxbaum, A. R., Wu, B. & Singer, R. H. Single β -actin mRNA detection in neurons reveals a
9 mechanism for regulating its translatability. *Science* **343**, 419–422 (2014).
- 10 48. Zhang, F., Saha, S., Shabalina, S. A. & Kashina, A. Differential arginylation of actin isoforms is
11 regulated by coding sequence-dependent degradation. *Science* **329**, 1534–1537 (2010).
- 12 49. Khaitlina, S. Y. Functional specificity of actin isoforms. *Int. Rev. Cytol.* **202**, 35–98 (2001).
- 13 50. Müller, M. *et al.* Distinct Functional Interactions between Actin Isoforms and Nonsarcomeric
14 Myosins. *PLOS ONE* **8**, e70636 (2013).
- 15 51. Yamaguchi, H. & Condeelis, J. Regulation of the actin cytoskeleton in cancer cell migration and
16 invasion. *Biochim. Biophys. Acta BBA - Mol. Cell Res.* **1773**, 642–652 (2007).
- 17 52. Izdebska, M., Zielińska, W., Hałas-Wiśniewska, M. & Grzanka, A. Involvement of Actin and Actin-
18 Binding Proteins in Carcinogenesis. *Cells* **9**, E2245 (2020).
- 19 53. Hall, A. The cytoskeleton and cancer. *Cancer Metastasis Rev.* **28**, 5–14 (2009).
- 20 54. Olson, M. F. & Sahai, E. The actin cytoskeleton in cancer cell motility. *Clin. Exp. Metastasis* **26**, 273
21 (2008).
- 22 55. Jia, S. *et al.* Down-regulation of WAVE2, WASP family verprolin-homologous protein 2, in gastric
23 cancer indicates lymph node metastasis and cell migration. *Anticancer Res.* **34**, 2185–2194 (2014).

- 1 56. Biber, G., Ben-Shmuel, A., Sabag, B. & Barda-Saad, M. Actin regulators in cancer progression and
2 metastases: From structure and function to cytoskeletal dynamics. *Int. Rev. Cell Mol. Biol.* **356**, 131–
3 196 (2020).
- 4 57. Morris, H. T. & Machesky, L. M. Actin cytoskeletal control during epithelial to mesenchymal
5 transition: focus on the pancreas and intestinal tract. *Br. J. Cancer* **112**, 613–620 (2015).
- 6 58. Lamouille, S., Xu, J. & Derynck, R. Molecular mechanisms of epithelial–mesenchymal transition. *Nat.*
7 *Rev. Mol. Cell Biol.* **15**, 178–196 (2014).
- 8 59. Piera-Velazquez, S. & Jimenez, S. A. Endothelial to Mesenchymal Transition: Role in Physiology and
9 in the Pathogenesis of Human Diseases. *Physiol. Rev.* **99**, 1281–1324 (2019).
- 10 60. Thiery, J. P., Acloque, H., Huang, R. Y. J. & Nieto, M. A. Epithelial-mesenchymal transitions in
11 development and disease. *Cell* **139**, 871–890 (2009).
- 12 61. Fritzsche, M., Lewalle, A., Duke, T., Kruse, K. & Charras, G. Analysis of turnover dynamics of the
13 submembranous actin cortex. *Mol. Biol. Cell* **24**, 757–767 (2013).
- 14 62. Molinie, N. & Gautreau, A. The Arp2/3 Regulatory System and Its Deregulation in Cancer. *Physiol.*
15 *Rev.* **98**, 215–238 (2018).
- 16 63. Schönichen, A. & Geyer, M. Fifteen formins for an actin filament: A molecular view on the regulation
17 of human formins. *Biochim. Biophys. Acta BBA - Mol. Cell Res.* **1803**, 152–163 (2010).
- 18 64. Jia, H., Yu, F., Li, B. & Gao, Z. Actin-binding protein Anillin promotes the progression of gastric cancer
19 in vitro and in mice. *J. Clin. Lab. Anal.* **35**, e23635 (2021).
- 20 65. Zhang, Y.-G. *et al.* Actin-Binding Proteins as Potential Biomarkers for Chronic Inflammation-Induced
21 Cancer Diagnosis and Therapy. *Anal. Cell. Pathol. Amst.* **2021**, 6692811 (2021).
- 22 66. Zhao, L. *et al.* Screening and clinical significance of tumor markers in head and neck squamous cell
23 carcinoma through bioinformatics analysis. *Mol. Med. Rep.* **19**, 143–154 (2019).

- 1 67. Dong, X., Han, Y., Sun, Z. & Xu, J. Actin Gamma 1, a new skin cancer pathogenic gene, identified by
2 the biological feature-based classification. *J. Cell. Biochem.* **119**, 1406–1419 (2018).
- 3 68. Ohtaki, S. *et al.* ACTC1 as an invasion and prognosis marker in glioma. *J. Neurosurg.* **126**, 467–475
4 (2017).
- 5 69. Popow, A., Nowak, D. & Malicka-Błaszkiwicz, M. Actin cytoskeleton and beta-actin expression in
6 correlation with higher invasiveness of selected hepatoma Morris 5123 cells. *J. Physiol. Pharmacol.*
7 *Off. J. Pol. Physiol. Soc.* **57 Suppl 7**, 111–123 (2006).
- 8 70. Suresh, R. *et al.* Expression of cell type incongruent alpha-cardiac actin 1 subunit in
9 medulloblastoma reveals a novel mechanism for cancer cell survival and control of migration.
10 *Neuro-Oncol. Adv.* **3**, vdab064 (2021).
- 11 71. Yang, M., Li, H., Li, Y., Ruan, Y. & Quan, C. Identification of genes and pathways associated with MDR
12 in MCF-7/MDR breast cancer cells by RNA-seq analysis. *Mol. Med. Rep.* **17**, 6211–6226 (2018).
- 13 72. da Rocha, R. G. *et al.* Leptin impairs the therapeutic effect of ionizing radiation in oral squamous cell
14 carcinoma cells. *J. Oral Pathol. Med. Off. Publ. Int. Assoc. Oral Pathol. Am. Acad. Oral Pathol.* **48**, 17–
15 23 (2019).
- 16 73. Huang, H.-C., Zheng, S., VanBuren, V. & Zhao, Z. Discovering disease-specific biomarker genes for
17 cancer diagnosis and prognosis. *Technol. Cancer Res. Treat.* **9**, 219–230 (2010).
- 18 74. Identification of Common Differentially Expressed Genes in Urinary Bladder Cancer | PLOS ONE.
19 <https://journals.plos.org/plosone/article?id=10.1371/journal.pone.0018135>.
- 20 75. Che, C.-L. *et al.* DNA microarray reveals different pathways responding to paclitaxel and docetaxel in
21 non-small cell lung cancer cell line. *Int. J. Clin. Exp. Pathol.* **6**, 1538–1548 (2013).
- 22 76. Li, Y., Rong, G. & Kang, H. Taxotere-induced elevated expression of IL8 in carcinoma-associated
23 fibroblasts of breast invasive ductal cancer. *Oncol. Lett.* **13**, 1856–1860 (2017).

- 1 77. Wanibuchi, M. *et al.* Actin, alpha, cardiac muscle 1 (ACTC1) knockdown inhibits the migration of
2 glioblastoma cells in vitro. *J. Neurol. Sci.* **392**, 117–121 (2018).
- 3 78. Valtz, N. L., Hayes, T. E., Norregaard, T., Liu, S. M. & McKay, R. D. An embryonic origin for
4 medulloblastoma. *New Biol.* **3**, 364–371 (1991).
- 5 79. Ramaswamy, V. *et al.* Risk stratification of childhood medulloblastoma in the molecular era: The
6 Current Consensus. *Acta Neuropathol. (Berl.)* **131**, 821–831 (2016).
- 7 80. Cavalli, F. M. G. *et al.* Intertumoral Heterogeneity within Medulloblastoma Subgroups. *Cancer Cell*
8 **31**, 737-754.e6 (2017).
- 9 81. Ramaswamy, V. & Taylor, M. D. Medulloblastoma: From Myth to Molecular. *J. Clin. Oncol.* **35**, 2355–
10 2363 (2017).
- 11 82. Liu, X., Ding, C., Tan, W. & Zhang, A. Medulloblastoma: Molecular understanding, treatment
12 evolution, and new developments. *Pharmacol. Ther.* **210**, 107516 (2020).
- 13 83. Northcott, P. A. *et al.* Medulloblastomics: The End of the Beginning. *Nat. Rev. Cancer* **12**, 818–834
14 (2012).
- 15 84. Millard, N. E. & De Braganca, K. C. Medulloblastoma. *J. Child Neurol.* **31**, 1341–1353 (2016).
- 16 85. Garcia-Lopez, J., Kumar, R., Smith, K. S. & Northcott, P. A. Deconstructing Sonic Hedgehog
17 Medulloblastoma: Molecular Subtypes, Drivers, and Beyond. *Trends Genet.* **37**, 235–250 (2021).
- 18 86. Gibson, P. *et al.* Subtypes of medulloblastoma have distinct developmental origins. *Nature* **468**,
19 1095–1099 (2010).
- 20 87. Jones, D. T. W. *et al.* Dissecting the genomic complexity underlying medulloblastoma. *Nature* **488**,
21 100–105 (2012).
- 22 88. Yang, Z.-J. *et al.* Medulloblastoma can be initiated by deletion of Patched in lineage-restricted
23 progenitors or stem cells. *Cancer Cell* **14**, 135–145 (2008).

- 1 89. Carballo, G. B., Honorato, J. R., de Lopes, G. P. F. & Spohr, T. C. L. de S. e. A highlight on Sonic
2 hedgehog pathway. *Cell Commun. Signal.* **16**, 11 (2018).
- 3 90. Fuccillo, M., Joyner, A. L. & Fishell, G. Morphogen to mitogen: the multiple roles of hedgehog
4 signalling in vertebrate neural development. *Nat. Rev. Neurosci.* **7**, 772–783 (2006).
- 5 91. Yam, P. T. & Charron, F. Signaling mechanisms of non-conventional axon guidance cues: the Shh,
6 BMP and Wnt morphogens. *Curr. Opin. Neurobiol.* **23**, 965–973 (2013).
- 7 92. Wechsler-Reya, R. J. & Scott, M. P. Control of Neuronal Precursor Proliferation in the Cerebellum by
8 Sonic Hedgehog. *Neuron* **22**, 103–114 (1999).
- 9 93. Huang, X. *et al.* Transventricular delivery of Sonic hedgehog is essential to cerebellar ventricular
10 zone development. *Proc. Natl. Acad. Sci. U. S. A.* **107**, 8422–8427 (2010).
- 11 94. Li, P. *et al.* A population of Nestin-expressing progenitors in the cerebellum exhibits increased
12 tumorigenicity. *Nat. Neurosci.* **16**, 1737–1744 (2013).
- 13 95. Liu, Y. *et al.* Astrocytes promote medulloblastoma progression through hedgehog secretion. *Cancer*
14 *Res.* **77**, 6692–6703 (2017).
- 15 96. Gronseth, E. *et al.* Astrocytes influence medulloblastoma phenotypes and CD133 surface expression.
16 *PLoS One* **15**, e0235852 (2020).
- 17 97. Cheng, Y. *et al.* Sustained hedgehog signaling in medulloblastoma tumoroids is attributed to stromal
18 astrocytes and astrocyte-derived extracellular matrix. *Lab. Investig. J. Tech. Methods Pathol.* **100**,
19 1208–1222 (2020).
- 20 98. Yao, M. *et al.* Astrocytic trans-Differentiation Completes a Multicellular Paracrine Feedback Loop
21 Required for Medulloblastoma Tumor Growth. *Cell* **180**, 502-520.e19 (2020).
- 22 99. Borah, N. A. & Reddy, M. M. Aurora Kinase B Inhibition: A Potential Therapeutic Strategy for Cancer.
23 *Molecules* **26**, 1981 (2021).

- 1 100. Marumoto, T., Zhang, D. & Saya, H. Aurora-A — A guardian of poles. *Nat. Rev. Cancer* **5**, 42–50
2 (2005).
- 3 101. Ghanizadeh-Vesali, S. *et al.* Significance of AZD1152 as a potential treatment against Aurora B
4 overexpression in acute promyelocytic leukemia. *Ann. Hematol.* **95**, 1031–1042 (2016).
- 5 102. Schwartz, G. K. *et al.* Phase I study of barasertib (AZD1152), a selective inhibitor of Aurora B
6 kinase, in patients with advanced solid tumors. *Invest. New Drugs* **31**, 370–380 (2013).
- 7 103. Diaz, R. J. *et al.* Mechanism of action and therapeutic efficacy of Aurora kinase B inhibition in
8 MYC overexpressing medulloblastoma. *Oncotarget* **6**, 3359–3374 (2014).
- 9 104. Pourcel, L. *et al.* Influence of cytoskeleton organization on recombinant protein expression by
10 CHO cells. *Biotechnol. Bioeng.* **117**, 1117–1126 (2020).
- 11 105. Despond, E. A. & Dawson, J. F. Classifying Cardiac Actin Mutations Associated With Hypertrophic
12 Cardiomyopathy. *Front. Physiol.* **9**, (2018).
- 13 106. Jiang, H.-K., Qiu, G.-R., Li-Ling, J., Xin, N. & Sun, K.-L. Reduced ACTC1 Expression Might Play a
14 Role in the Onset of Congenital Heart Disease by Inducing Cardiomyocyte Apoptosis. *Circ. J.* **74**,
15 2410–2418 (2010).
- 16 107. Mundia, M. M., Demers, R. W., Chow, M. L., Perieteanu, A. A. & Dawson, J. F. Subdomain
17 Location of Mutations in Cardiac Actin Correlate with Type of Functional Change. *PLOS ONE* **7**,
18 e36821 (2012).
- 19 108. Do cardiac actin mutations lead to altered actomyosin interactions?
20 [https://cdnsiencepub.com/doi/full/10.1139/bcb-2014-](https://cdnsiencepub.com/doi/full/10.1139/bcb-2014-0156?casa_token=0I2RtPgXVsOAAAAA%3ASXfy7vLxw__VjicJkiutemRCpsTke1Frnx_GOzDGfC3bOU)
21 [0156?casa_token=0I2RtPgXVsOAAAAA%3ASXfy7vLxw__VjicJkiutemRCpsTke1Frnx_GOzDGfC3bOU](https://cdnsiencepub.com/doi/full/10.1139/bcb-2014-0156?casa_token=0I2RtPgXVsOAAAAA%3ASXfy7vLxw__VjicJkiutemRCpsTke1Frnx_GOzDGfC3bOU)
22 [Gqwk6YjCsrojGJ2i2XzUsosRKHHq.](https://cdnsiencepub.com/doi/full/10.1139/bcb-2014-0156?casa_token=0I2RtPgXVsOAAAAA%3ASXfy7vLxw__VjicJkiutemRCpsTke1Frnx_GOzDGfC3bOU)
- 23 109. Rangrez, A. Y. *et al.* Data on the role of cardiac α -actin (ACTC1) gene mutations on SRF-signaling.
24 *Data Brief* **28**, 105071 (2020).

- 1 110. Nattel, S. N. *et al.* Congenital Heart Disease and Neurodevelopment: Clinical Manifestations,
2 Genetics, Mechanisms, and Implications. *Can. J. Cardiol.* **33**, 1543–1555 (2017).
- 3 111. Zaidi, S. & Brueckner, M. Genetics and Genomics of Congenital Heart Disease. *Circ. Res.* **120**,
4 923–940 (2017).
- 5 112. Hsu, P. *et al.* CHARGE syndrome: a review. *J. Paediatr. Child Health* **50**, 504–511 (2014).
- 6 113. McDonald-McGinn, D. M. *et al.* 22q11.2 deletion syndrome. *Nat. Rev. Dis. Primer* **1**, 15071
7 (2015).
- 8 114. Homans, J. F. *et al.* The role of 22q11.2 deletion syndrome in the relationship between
9 congenital heart disease and scoliosis. *Spine J. Off. J. North Am. Spine Soc.* **20**, 956–963 (2020).
- 10 115. Gao, S., Li, X. & Amendt, B. A. Understanding the role of Tbx1 as a candidate gene for 22q11.2
11 deletion syndrome. *Curr. Allergy Asthma Rep.* **13**, 613–621 (2013).
- 12 116. Jacobsen, P. F., Jenkyn, D. J. & Papadimitriou, J. M. Establishment of a human medulloblastoma
13 cell line and its heterotransplantation into nude mice. *J. Neuropathol. Exp. Neurol.* **44**, 472–485
14 (1985).
- 15 117. Keles, G. E. *et al.* Establishment and characterization of four human medulloblastoma-derived
16 cell lines. *Oncol. Res.* **7**, 493–503 (1995).
- 17 118. Lee, H. Y., Greene, L. A., Mason, C. A. & Manzini, M. C. Isolation and culture of post-natal mouse
18 cerebellar granule neuron progenitor cells and neurons. *J. Vis. Exp. JoVE* 990 (2009)
19 doi:10.3791/990.
- 20 119. Goggolidou, P. *et al.* A chronological expression profile of gene activity during embryonic mouse
21 brain development. *Mamm. Genome Off. J. Int. Mamm. Genome Soc.* **24**, 459–472 (2013).
- 22 120. Schüller, U. *et al.* Acquisition of granule neuron precursor identity is a critical determinant of
23 progenitor cell competence to form Shh-induced medulloblastoma. *Cancer Cell* **14**, 123–134 (2008).

- 1 121. Skowron, P. *et al.* The transcriptional landscape of Shh medulloblastoma. *Nat. Commun.* **12**,
2 1749 (2021).
- 3 122. Micheva, K. D., Vallée, A., Beaulieu, C., Herman, I. M. & Leclerc, N. beta-Actin is confined to
4 structures having high capacity of remodelling in developing and adult rat cerebellum. *Eur. J.*
5 *Neurosci.* **10**, 3785–3798 (1998).
- 6 123. Murthy, K. & Wadsworth, P. Myosin-II-dependent localization and dynamics of F-actin during
7 cytokinesis. *Curr. Biol. CB* **15**, 724–731 (2005).
- 8